iScience

CellPress

Article

Nonmetallic Abiotic-Biological Hybrid Photocatalyst for Visible Water Splitting and Carbon Dioxide Reduction

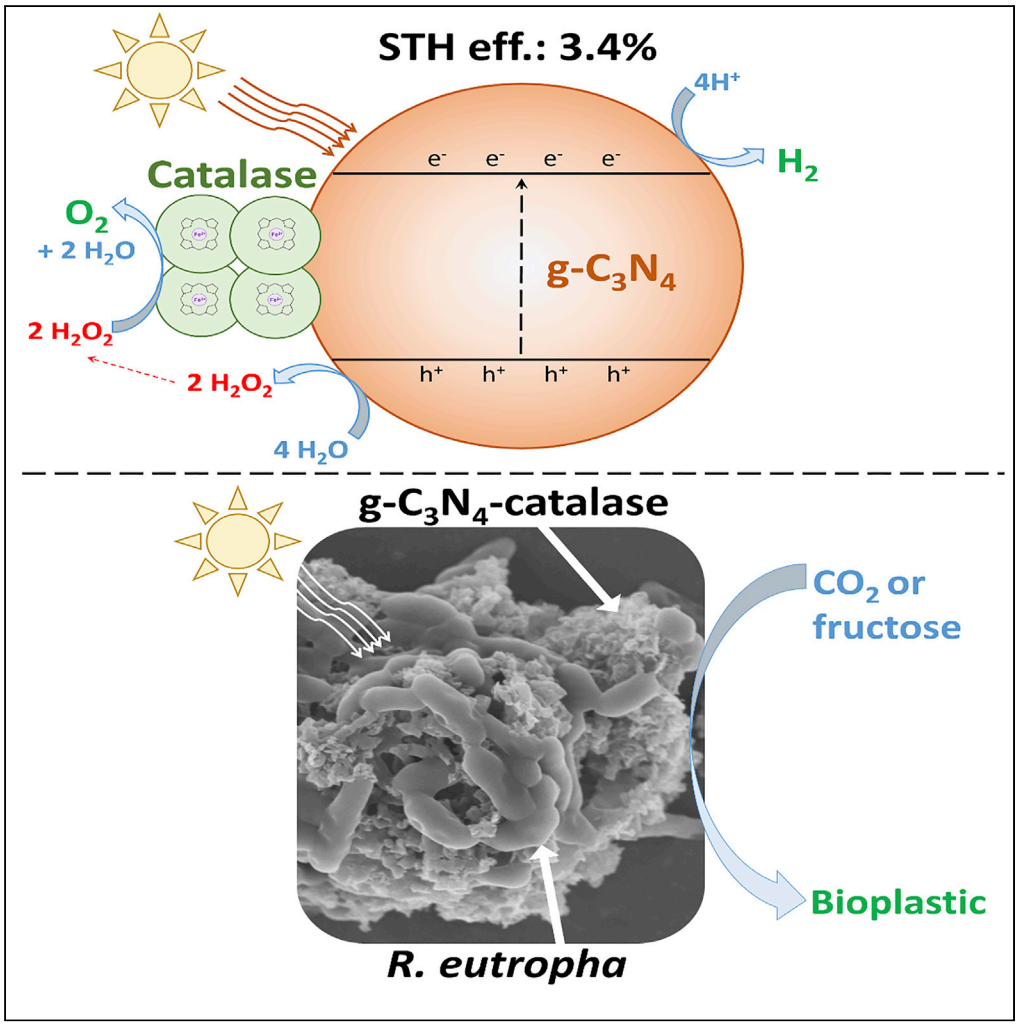

Pier-Luc Tremblay, Mengying Xu, Yiming Chen, Tian Zhang

tzhang@whut.edu.cn

HIGHLIGHTS

H_2O_2-degrading enzymes from *R. eutropha* enable visible-light water splitting by C_3N_4

C_3N_4 coupled with bovine catalase has a solar-to-hydrogen efficiency of 3.4%

C_3N_4-catalase increases CO_2 conversion into bioplastic under light by *R. eutropha*

Heterotrophic bioplastic production by *R. eutropha* is also improved by C_3N_4-catalase

Tremblay et al., iScience *23*, 100784
January 24, 2020
https://doi.org/10.1016/j.isci.2019.100784

iScience

CellPress

Article

Nonmetallic Abiotic-Biological Hybrid Photocatalyst for Visible Water Splitting and Carbon Dioxide Reduction

Pier-Luc Tremblay,[1,2,5] Mengying Xu,[1,2,3,5] Yiming Chen,[4] and Tian Zhang[1,2,3,6,*]

SUMMARY

Both artificial photosystems and natural photosynthesis have not reached their full potential for the sustainable conversion of solar energy into specific chemicals. A promising approach is hybrid photosynthesis combining efficient, non-toxic, and low-cost abiotic photocatalysts capable of water splitting with metabolically versatile non-photosynthetic microbes. Here, we report the development of a water-splitting enzymatic photocatalyst made of graphitic carbon nitride (g-C_3N_4) coupled with H_2O_2-degrading catalase and its utilization for hybrid photosynthesis with the non-photosynthetic bacterium *Ralstonia eutropha* for bioplastic production. The g-C_3N_4-catalase system has an excellent solar-to-hydrogen efficiency of 3.4% with a H_2 evolution rate up to 55.72 μmol h^{-1} while evolving O_2 stoichiometrically. The hybrid photosynthesis system built with the water-spitting g-C_3N_4-catalase photocatalyst doubles the production of the bioplastic polyhydroxybutyrate by *R. eutropha* from CO_2 and increases it by 1.84-fold from fructose. These results illustrate how synergy between abiotic non-metallic photocatalyst, enzyme, and bacteria can augment solar-to-multicarbon chemical conversion.

INTRODUCTION

Multiple technologies are being developed to convert and store solar energy, which is not only ubiquitous, sustainable, and clean but also intermittent. Artificial water-splitting photosystems have attracted interest mainly for the production of storable H_2 from sunlight (Chen et al., 2017). The three main types of abiotic photosystems for H_2 production are photovoltaic cell coupled with electrolyzer (PV-E), photoelectrochemical cell (PEC), and particulate photocatalyst (PC) (Chen et al., 2017). PV-E has shown the highest solar-to-hydrogen (STH) conversion efficiency, but H_2 production cost by PV-E is not competitive with already established industrial processes. Between PEC and PC, techno-economical assessments conclude that PC would have a lower H_2 production cost, as little as \$1.60 kg^{-1} when similar STH efficiencies are considered (Pinaud et al., 2013). Compared with PV-E and PEC, PC is a simpler system more suitable for low-cost scaling up. However, STH efficiencies reported until now for PC and PEC are lower than those reported for PV-E (Chen et al., 2017; Prévot and Sivula, 2013). Another important challenge is that, with scarce exceptions, the most efficient PC systems are made with expensive rare-earth elements (Liu et al., 2015a).

A promising solar technology is hybrid photosynthesis where an abiotic photosystem converts sunlight into chemical energy and transfers it to microbes for the production of multicarbon chemicals (Zhang and Tremblay, 2017). In these systems, chemical energy from the abiotic photosystem can drive or accelerate either autotrophic or heterotrophic bioproduction processes (Xu et al., 2019; Zhang et al., 2018; Liu et al., 2015b, 2016; Sakimoto et al., 2016a, 2016b; Guo et al., 2018; Nichols et al., 2015; Ye et al., 2019). In its autotrophic configuration where the greenhouse gas CO_2 is the carbon source, hybrid photosynthesis will mirror natural photosynthesis carried out by living organisms if electrons come from water splitting. Hybrid photosynthesis is being pursued owing to the abiotic photosystems that are significantly more efficient at converting solar energy into chemical energy than natural photosynthesis. Thus, coupling abiotic photosystems with productive microbial catalysts may outcompete natural photosynthesis in terms of solar-to-specific chemicals efficiency (Zhang, 2015; Tremblay et al., 2017; Claassens et al., 2016).

Graphitic carbon nitride (g-C_3N_4) is a metal-free low-cost PC, easy to fabricate, and made of earth-abundant elements with a band gap of 2.7 eV that can convert solar energy into H_2 (Liu et al., 2015a; Wang et al., 2009; Yan et al., 2010; Rao et al., 2019). Other applications of g-C_3N_4 include light-driven pollutant remediation and CO_2 reduction into other C1 compounds (Hu et al., 2014; Ye et al., 2015; Zhang et al.,

[1]State Key Laboratory of Silicate Materials for Architectures, Wuhan University of Technology, Wuhan 430070, PR China

[2]School of Chemistry, Chemical Engineering and Life Science, Wuhan University of Technology, Wuhan 430070, PR China

[3]School of Materials Science and Engineering, Wuhan University of Technology, Wuhan 430070, PR China

[4]State Key Laboratory of Advanced Technology for Materials Synthesis and Processing, Wuhan University of Technology, Wuhan 430070, PR China

[5]These authors contributed equally

[6]Lead Contact

*Correspondence: tzhang@whut.edu.cn

https://doi.org/10.1016/j.isci.2019.100784

2015; Mishra et al., 2019a; Reddy et al., 2019). Recently, a hybrid photosynthesis system was developed with g-C_3N_4 where the production of the bioplastic polyhydroxybutyrate (PHB) from fructose by *Ralstonia eutropha* H16 was enhanced under light (Xu et al., 2019). *R. eutropha* is an aerobic bacterium also known as *Cupriviadus necator* that can grow heterotrophically or autotrophically with CO_2 as carbon source and H_2 or an electrode as electron donor (Liu et al., 2016; Tanaka et al., 1995; Li et al., 2012; Volodina et al., 2016). One of the main appeals of *R. eutropha* as a microbial factory is that it stores intracellularly large quantity of PHB when carbon is in excess (Tanaka et al., 1995). *R. eutropha* can also be genetically engineered to redirect metabolic fluxes toward the synthesis of a wide range of valuable chemicals (Li et al., 2012; Bi et al., 2013; Chakravarty and Brigham, 2018; Grousseau et al., 2014; Lu et al., 2012; Müller et al., 2013).

Most pristine g-C_3N_4 materials without modifications are unable to evolve H_2 in the absence of sacrificial electron donors (SED) such as triethanolamine (TEOA), methanol, or lactic acid (Wang et al., 2017). Photocatalytic water splitting by g-C_3N_4 and resulting H_2 and O_2 evolution is theoretically possible but is hindered by sluggish kinetics (Zhang et al., 2016; Mishra et al., 2019b). Recently, a study by Fang et al. described a g-C_3N_4 photocatalyst prepared by an alternative method from a cocrystal precursor capable of using H_2O as electron donor for H_2 evolution (Fang et al., 2019). The authors attributed the water-splitting capacity of their PC to improved generation and mobility of the photoexcited charge carriers. One of the main obstacles for light-driven water splitting by g-C_3N_4 involves the O_2 evolution reaction, which necessitates the transfer of four electrons and four protons for the formation of a double bond between two oxygen molecules ($2H_2O \rightarrow 4H^+ + 4e^- + O_2$, 1.23 eV). With g-$C_3N_4$, the four-electron reaction for O_2 evolution has been shown to be outcompeted kinetically by a two-electron reaction wherein H_2O is oxidized into H_2O_2 ($2H_2O \rightarrow 2H^+ + 2e^- + H_2O_2$, 1.78 eV) (Liu et al., 2012). This phenomenon inhibits O_2 and H_2 evolution reactions because H_2O_2 deactivates g-C_3N_4 by staying attached to it and by occupying active surface sites. A solution reported in the past to overcome H_2O_2 poisoning and complete O_2 and H_2 evolution is to modify g-C_3N_4 PC with carbon nanodots (CDots), which have good catalytic activity for H_2O_2 degradation (Liu et al., 2015a).

In a previous study, we showed that no SED was required for unmodified g-C_3N_4 to augment heterotrophic PHB production by *R. eutropha* under light (Xu et al., 2019). Possible explanations are that *R. eutropha* modifies the growth medium surrounding g-C_3N_4 or its surface in a way that improves g-C_3N_4's photocatalytic performance and/or enables water splitting. To understand the mechanisms involved, we investigated the photocatalytic performance and behavior of g-C_3N_4 suspended in cell-free spent medium from *R. eutropha*. The results indicated that H_2O_2-degrading enzymes present in the spent medium were degrading the H_2O_2 generated by g-C_3N_4 under light, and thus enabled photocatalytic water splitting. Based on these observations, we developed a novel PC system coupling g-C_3N_4 with pure bovine liver catalase, which is an enzyme specialized in the degradation of H_2O_2 into O_2 and H_2O. This novel g-C_3N_4-catalase PC system was employed to build a hybrid photosynthesis system where the production of PHB from either CO_2 or fructose by *R. eutropha* was driven by water-splitting photocatalysis.

RESULTS

H_2O_2-Degrading Enzymes from the Spent Medium of *R. eutropha* and Faster Hydrogen Evolution by Unmodified g-C_3N_4

To establish how g-C_3N_4 was active under light when coupled with *R. eutropha* for PHB production in the absence of SEDs (Xu et al., 2019), fructose-grown *R. eutropha* cells were removed from the growth medium by centrifugation, g-C_3N_4 (Figures S1 and S2) was added to the cell-free spent medium, and light-driven H_2 evolution was monitored under light-emitting diode (LED) light (Figure 1A). g-C_3N_4 in the cell-free spent medium had a H_2 evolution rate (HER) of 0.57 $\pm$ 0.05 μmol h^{-1} (57.4 $\pm$ 4.7 μmol g^{-1} h^{-1}), which was 16.4 times higher than that of pristine growth medium and 2.1 times higher than that of pristine growth medium with 0.5% TEOA. Next, cell-free spent medium was treated with the protease mixture pronase to establish if the compound responsible for improved HER was a protein or a group of proteins (Figure 1B). With pronase-treated cell-free spent medium, HER was significantly reduced to 0.06 $\pm$ 0.01 μmol h^{-1} (5.8 $\pm$ 1.2 μmol g^{-1} h^{-1}), which is comparable to HER observed with pristine medium. Thus, the compound(s) in cell-free spent medium accelerating light-driven HER by g-C_3N_4 is proteinaceous.

Besides HER, concentrations of the O_2 evolution inhibitor H_2O_2 were also monitored when g-C_3N_4 was exposed to light in pristine growth medium and cell-free spent medium (Figure 2A). In pristine medium containing g-C_3N_4, H_2O_2 accumulated in a light-dependent manner up to 20.9 $\pm$ 4.7 μmol after 1 h. In

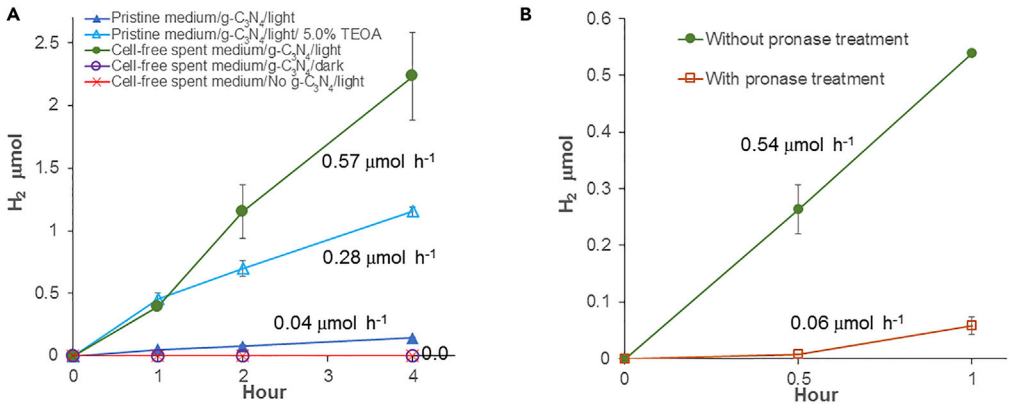

Figure 1. Light-Driven H_2 Evolution by g-C_3N_4 in *R. eutropha* Spent Medium

(A) H_2 evolution by g-C_3N_4 in pristine medium and cell-free spent medium under light. Where indicated, 5.0% TEOA was added.

(B) H_2 evolution by g-C_3N_4 in cell-free spent medium treated with/without pronase under light. Each curve is the mean and standard deviation of at least three replicates.

comparison, no H_2O_2 accumulated with cell-free spent medium, which probably explained why HER was significantly higher under this condition.

Many organisms including bacteria have an enzymatic mechanism to defend themselves against H_2O_2, which can cause extensive oxidative damages (Mishra and Imlay, 2012). Two enzymes ubiquitous in aerobic organisms are responsible for biological H_2O_2 degradation: the catalase and the peroxidase. Catalases degrade H_2O_2 according to the following equation: $2\ H_2O_2 \rightarrow 2\ H_2O + O_2$ (Mishra and Imlay, 2012). Peroxidases require a physiological electron donor such as thioredoxins, glutathione NAD(P)H, or cytochrome *c* to reduce H_2O_2 according to the following equation: $RH_2 + H_2O_2 \rightarrow R + 2H_2O$. The genome of *R. eutropha* H16 comprises at least nine genes coding for catalases and peroxidases (Table S1) (Pohlmann et al., 2006). Results presented here strongly suggest that some of these enzymes are located in the cell-free spent medium of *R. eutropha*, either because of excretion or cell lysis, where they degraded H_2O_2 and increased HER by g-C_3N_4. In fact, when exogenous H_2O_2 was added to cell-free spent medium, it was degraded at a rate of 203.6 $\pm$ 16.7 nmol min^{-1} mL^{-1} or 9.1 $\pm$ 0.3 µmol min^{-1} per mg protein in the spent medium, whereas no degradation was observed in pristine medium (Figure 2B).

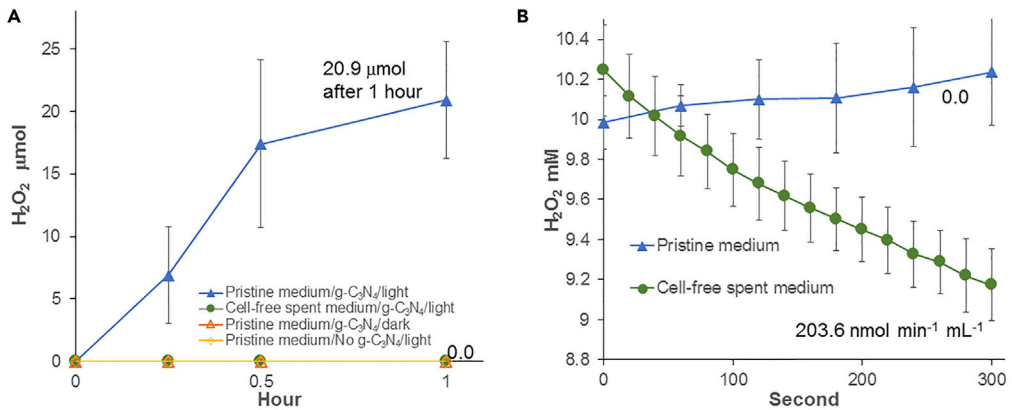

Figure 2. H_2O_2 Generation by g-C_3N_4 and Degradation by *R. eutropha* Spent Medium

(A) H_2O_2 generation by g-C_3N_4.

(B) H_2O_2-degrading activity in *R. eutropha* spent medium amended with 10 mM H_2O_2. Each curve is the mean and standard deviation of at least three replicates.

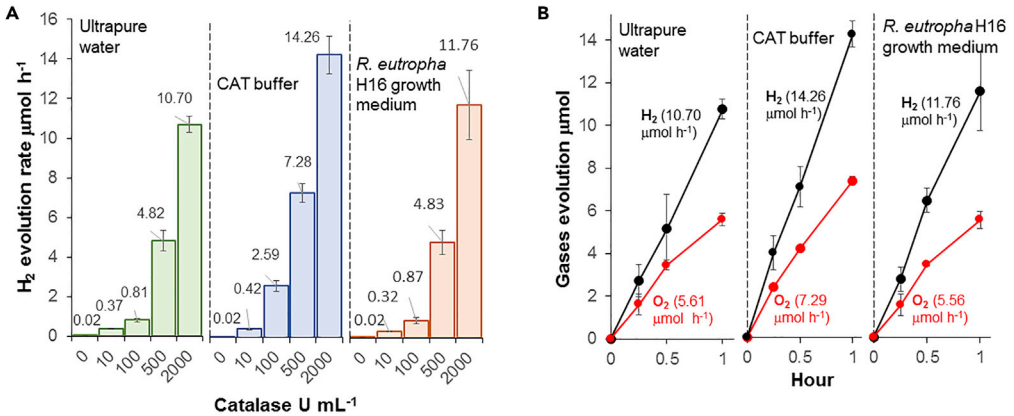

Figure 3. Light-Driven Water-Splitting Activity of the g-C_3N_4-Catalase System

(A) Impact of bovine liver catalase concentration on H_2 evolution rate by g-C_3N_4 suspended in ultrapure water, CAT buffer, or *R. eutropha* growth medium under 4,200-lux LED light.

(B) H_2 and O_2 evolution under 4,200-lux LED light over time by g-C_3N_4 with 2,000 U mL^{-1} catalase. Each curve and bar is the average of at least three replicates with standard deviation.

A Water-Splitting Photocatalytic System Coupling g-C_3N_4 and Pure Catalase

To investigate further the impact of H_2O_2-degrading enzymes on the photocatalytic activity of g-C_3N_4, the performance of g-C_3N_4 loaded with different quantity of bovine liver catalase was evaluated in ultrapure water, in catalase buffer (CAT buffer; 50 mM KH_2PO_4 pH 7.4), and in pristine *R. eutropha* growth medium (Figures 3 and S3–S5). Under LED light, increasing the quantity of catalase within the three types of suspension resulted in significant H_2 production by g-C_3N_4 up to 14.26 ± 1.00 µmol h^{-1} (1,426.4 ± 95.9 µmol g^{-1} h^{-1}) with 2,000 U mL^{-1} catalase in CAT buffer. H_2 production was accompanied by nearly stoichiometric O_2 evolution of 7.29 ± 0.19 µmol h^{-1} (729.5 ± 18.5 µmol g^{-1} h^{-1}) demonstrating light-driven water splitting by the enzymatic PC system (Figure 3B). In the absence of catalase, O_2 evolution was not detected in ultrapure water, CAT buffer, or growth medium, indicating that the presence of the enzyme not only accelerated H_2 evolution but also enabled O_2 evolution. Besides O_2 and H_2 evolution, H_2O_2 accumulation was also monitored with the PC system coupling g-C_3N_4 with 2,000 U ml^{-1} catalase under light. With all three different suspensions, no H_2O_2 was detected, showing that the catalase degraded its substrate and prevented the buildup of this reactive oxygen species.

The addition of 100 U ml^{-1} superoxide dismutase (SOD) to g-C_3N_4 instead of catalase did not improve H_2 production with a rate of 0.01 ± 0.00 µmol h^{-1} (1.5 ± 0.2 and 1.2 ± 0.2 µmol g^{-1} h^{-1}) in both ultrapure water and growth medium (Figure S6). Under similar light condition, pure g-C_3N_4 had a H_2 production rate of 0.02 µmol h^{-1} (2.0 µmol g^{-1} h^{-1}) in both ultrapure water and growth medium (Figure 3A). At the same concentration of 100 U ml^{-1}, catalase already significantly improved H_2 evolution by g-C_3N_4 to 0.81 ± 0.09 and 0.87 ± 0.15 µmol h^{-1} (81.2 ± 8.6 and 87.1 ± 14.5 µmol g^{-1} h^{-1}) in ultrapure water and growth medium, respectively. Like the catalase, SOD is an enzyme participating in living cells' defense against oxidative stress (Johnson and Hug, 2019). SOD catalyzes the conversion of superoxide into O_2 and H_2O_2. These results clearly suggest that the increased H_2 production observed with the g-C_3N_4-catalase PC system was caused by the enzymatic activity of the catalase and not by an unspecific effect related to the addition of enzymes or proteins independently of their capacity to degrade H_2O_2.

The energetic efficiency of the novel g-C_3N_4-catalase system was evaluated with 2,000, 5,000, and 10,000 U mL^{-1} bovine liver catalase in CAT buffer under an AM 1.5G solar simulator with a light intensity of 200 or 800 W m^{-2} (*ca.* 0.2 or 0.8 sun) (Figure 4). The highest STH efficiency of 3.40% ± 0.2% was recorded with 10,000 U mL^{-1} catalase at a light intensity of 200 W m^{-2}. For this experiment, the irradiated surface was 4.6 cm^2 for a total input energy in 1 h of 331.2 J. H_2 production was 47.49 ± 0.32 µmol, which amounted to 11.26 J. At 5,000 U mL^{-1} catalase, the STH efficiency was statistically similar at 3.12% ± 0.69%, but it became 1.88 times lower when catalase concentration was reduced to 2,000 U mL^{-1}. Increasing light intensity to 800 W m^{-2} augmented HER while reducing STH efficiency. The best PC system at 800 W m^{-2} had a catalase concentration of 5,000 U mL^{-1} with an STH efficiency of 1.00% ± 0.19% and a normalized HER of 55.72 ± 10.40 µmol h^{-1} (1,857.16 ± 346.72 µmol g^{-1} h^{-1}). O_2 evolution for all tested conditions

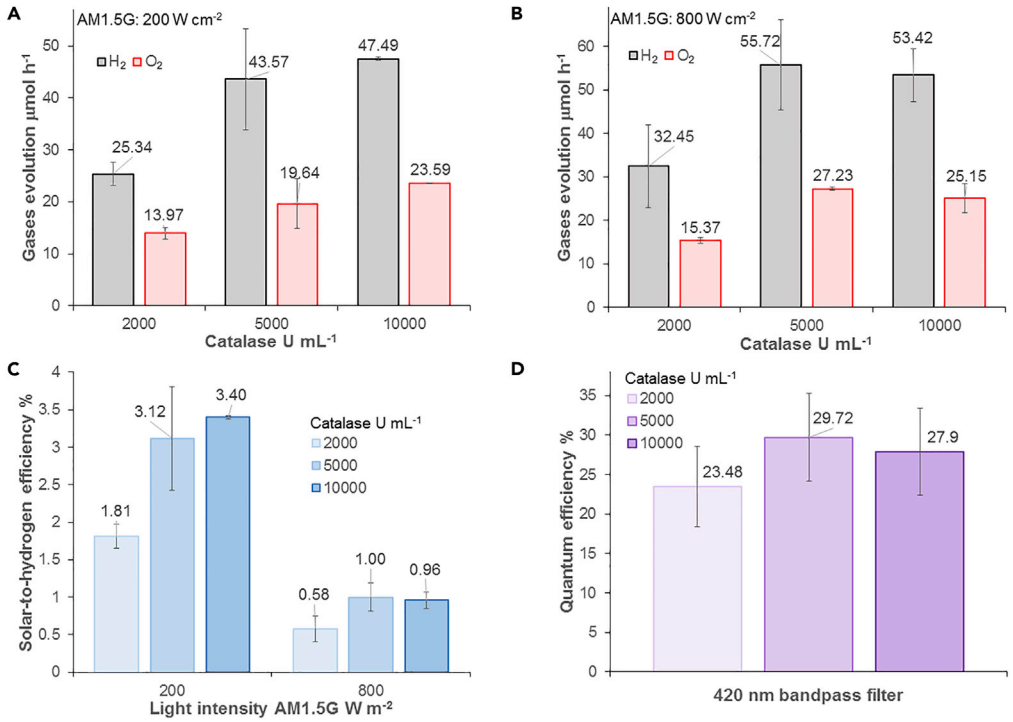

Figure 4. H_2 Evolution and O_2 Evolution by g-C_3N_4-Catalase under an AM1.5G

(A) Gases evolution at a light intensity of 200 W m^{-2}. (B) Gases evolution at a light intensity of 800 W m^{-2}.
(C and D) (C) Solar-to-hydrogen efficiency and (D) quantum efficiency at 420 nm for the g-C_3N_4-catalase PC system. Each curve and bar is the average of at least three replicates with standard deviation.

was nearly stoichiometric (Figures 4A and 4B). Quantum efficiency at a wavelength of 420 nm, which is in the optimal absorption spectrum for g-C_3N_4, was 23.48% ± 5.06% with 2,000 U mL^{-1} catalase, 29.72% ± 5.53% with 5,000 U mL^{-1} catalase, and 27.90% ± 5.50% with 10,000 U mL^{-1} catalase (Figure 4D). STH efficiencies at low light intensity for the g-C_3N_4-catalase PC system described here are higher than CDots-C_3N_4 PC, which is, with an efficiency of 2%, one of the best reported water-splitting photocatalysts (Table S2) (Liu et al., 2015a). In addition, the g-C_3N_4-based PC system was stable when tested with 10,000 U mL^{-1} catalase under a light intensity of 200 W m^{-2} (Figure S7). After three cycles, H_2 and O_2 evolution rates were comparable to the initial rates.

Hybrid Photosynthesis with g-C_3N_4-Catalase and *R. eutropha* for CO_2 Reduction

Autotrophic hybrid photosynthesis apparatuses developed until now rely on metallic inorganic PC harvesting visible light to drive biological CO_2 reduction by non-photosynthetic bacteria (Table S3) (Zhang and Tremblay, 2017; Zhang et al., 2018; Sakimoto et al., 2016a; Ye et al., 2019). Most of these systems photogenerated the reducing equivalents ultimately transferred to the autotrophic microbe by the oxidation of an SED such as cysteine. In these circumstances, the requirement for an SED diminishes significantly the sustainability prospect of PC-based bioprocesses. Only one hybrid photosynthesis system reported until now relies on water splitting and not on an SED (Sakimoto et al., 2016b). This tandem "Z-scheme" platform included potentially toxic TiO_2 combined with the cocatalyst Mn(II) phthalocyanine photo-oxidizing water and transferring the electrons indirectly to CdS via a cysteine shuttle. CdS then photogenerated reducing equivalents, which were carried out to the acetogen *Moorella thermoacetica* for the reduction of CO_2 into acetate.

To establish if the water-splitting g-C_3N_4-catalase PC system developed here could provide energy for autotrophic bioproduction process, it was coupled with *R. eutropha* growing autotrophically under a N_2:H_2:CO_2:O_2 atmosphere and synthesis of PHB was monitored (Figure 5A). With g-C_3N_4-catalase, PHB production from CO_2 under light reached 41.02 ± 6.22 mg L^{-1} after 48 h compared

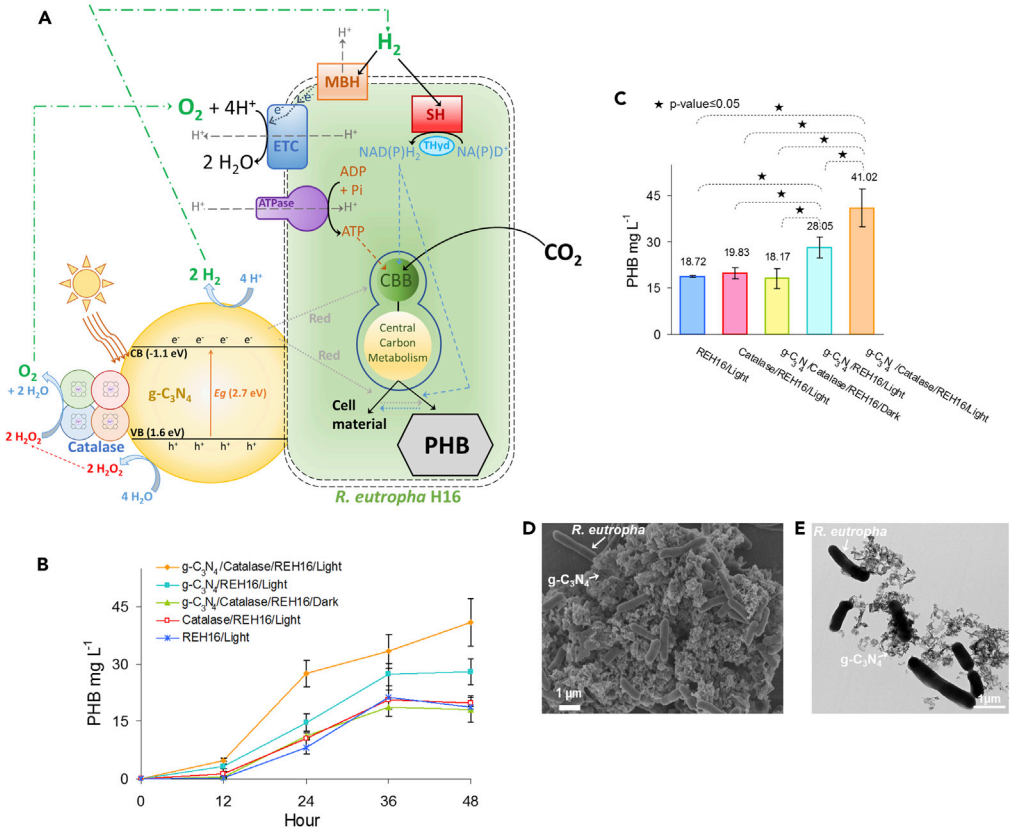

Figure 5. Autotrophic Hybrid Photosynthesis with g-C_3N_4-Catalase and *R. eutropha*

(A) Schematic diagram of hybrid photosynthesis with g-C_3N_4-catalase and *R. eutropha* producing PHB from CO_2. Water-splitting g-C_3N_4-catalase could augment PHB production either by increasing the quantity of H_2 and/or O_2 available for bacterial metabolism or by transferring unknown reducing equivalents (red) to *R. eutropha*. CB, conduction band; VB, valence band; ETC, electron transport chain; MBH, membrane-bound hydrogenase; SH, soluble hydrogenase; Thyd, $NAD(P)^+$ transhydrogenase; CBB, Calvin-Benson-Bassham cycle (Brigham et al., 2013).

(B and C) (B) PHB production from CO_2 over time and (C) PHB concentration after 48 h. REH16, *R. eutropha* H16.

(D and E) (D) Scanning and (E) transmission electron micrographs of *R. eutropha* grown with g-C_3N_4-catalase under autotrophic condition. *R. eutropha* cultures were grown at 30 ºC in minimal medium under a N_2:H_2:O_2:CO_2 (49:37:7:7) atmosphere in the presence or absence 0.5 g g-C_3N_4 and/or 5,000 U mL^{-1} bovine liver catalase. Where indicated, cultures were incubated under 4,200-lux LED light. Each curve and bar is the mean of at least three replicates with standard deviation.

with 18.72 ± 0.31mg L^{-1} for a light-exposed *R. eutropha* culture grown without the PC system (Figures 5B and 5C). Both scanning electron microscopy and transmission electron microscopy images showed the formation of large aggregates under autotrophic conditions with direct physical contact between g-C_3N_4 particles and *R. eutropha* cells (Figures 5D, 5E, and S8). Bovine liver catalase was not required for g-C_3N_4 to improve autotrophic PHB production, but the addition of the enzyme still had a significant positive effect. g-C_3N_4 without catalase augmented PHB production from CO_2 by *R. eutropha* to 28.05 ± 3.37 mg L^{-1} under light. This can be explained by native H_2O_2-degrading enzymes possibly released by *R. eutropha* cells, which enables water splitting by g-C_3N_4, but not to the same level as with bovine liver catalase.

Production improvement observed with g-C_3N_4-catalase was light-dependent. *R. eutropha* with g-C_3N_4-catalase in the dark produced only 18.17 ± 3.29 mg L^{-1} PHB after 48 h (Figures 5B and 5C). The addition of 5,000 U mL^{-1} catalase alone without g-C_3N_4 did not improve PHB production, which demonstrates that *R. eutropha* cells could not use the enzyme as substrate for their metabolism.

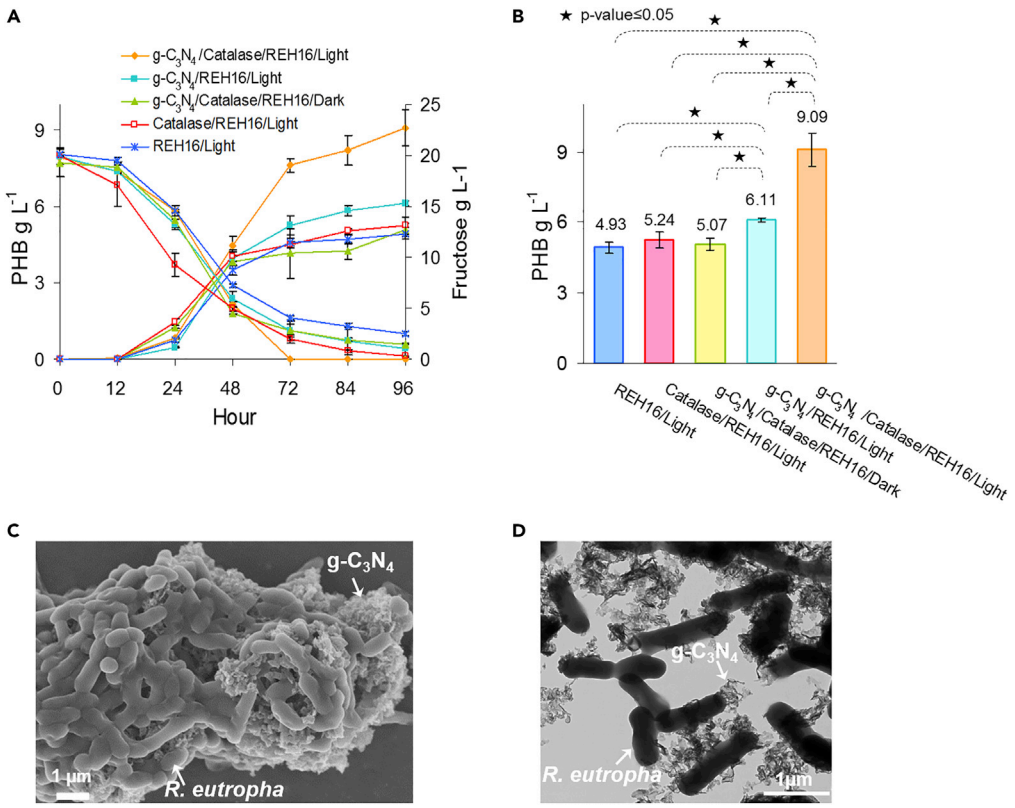

Figure 6. Heterotrophic Hybrid Photosynthesis with g-C_3N_4-Catalase and *R. eutropha*

(A and B) (A) PHB production and fructose consumption over time and (B) PHB concentration after 96 h.
(C and D) (C) Scanning and (D) transmission electron micrographs of *R. eutropha* grown with g-C_3N_4-catalase under heterotrophic conditions. *R. eutropha* cultures were grown at 30 ºC in minimal medium with 20 g L^{-1} fructose in the presence or absence 0.5 g g-C_3N_4 and/or 5,000 U mL^{-1} bovine liver catalase. Where indicated, cultures were incubated under 4,200-lux LED light. Each curve and bar is the mean of at least three replicates with standard deviation.

The increase of PHB production observed with the photocatalytic system during autotrophic growth of *R. eutropha* may have three possible explanations (Figure 5A). First, H_2 initially provided in the gas phase to drive bacterial growth may become scarcer after biological oxidation. g-C_3N_4-catalase generates supplementary H_2 used by *R. eutropha* to keep its metabolism active, which results in additional PHB production. Second, O_2 may also become rarer in the gas phase after bacterial reduction during growth. While generating reducing equivalents, g-C_3N_4-catalase also evolves additional O_2 by water splitting that can be used by the bacterial cells as electron acceptor. Third, the photocatalytic system may transfer electrons directly to *R. eutropha* or generate reducing equivalents under a different form than H_2 that are preferentially used by the bacteria.

Heterotrophic Production of PHB from Fructose with g-C_3N_4-Catalase

The impact of the g-C_3N_4-catalase system on heterotrophic production of PHB from fructose by *R. eutropha* was also evaluated (Figure S9). As reported previously (Xu et al., 2019), the addition of g-C_3N_4 alone is sufficient to improve PHB production from fructose under light with a 124% increase compared with an *R. eutropha* culture without g-C_3N_4 (Figures 6A, 6B, and S10). The only other example where heterotrophic bioproduction was enhanced by a light-harvesting photocatalyst coupled the rare element indium phosphide with a *Saccharomyces cerevisiae* strain producing shikimate from glucose (Guo et al., 2018). When the g-C_3N_4-catalase system developed here was combined with *R. eutropha*, PHB production reached 9.09 $\pm$ 0.71 g L^{-1} after 96 h of growth under light, which was 1.84-fold higher compared with heterotrophic *R. eutropha* without the PC system. Large aggregates with direct physical contact between g-C_3N_4 and *R. eutropha* cells were also observed in the heterotrophic mode (Figures 6C and 6D). Fructose-grown *R. eutropha* control with catalase only and no g-C_3N_4 under light as well as

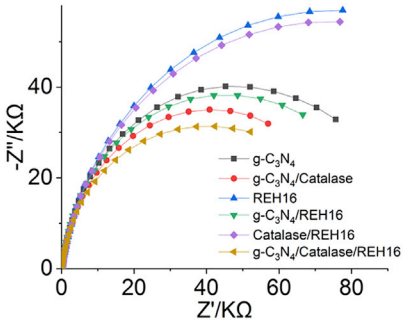

Figure 7. Electrochemical Impedance Spectroscopy of the Autotrophic Hybrid Photosynthesis System under Light

a control grown in the dark with the g-C_3N_4-catalase system had PHB production comparable to *R. eutropha* without g-C_3N_4 and catalase (Figures 6A and 6B).

Charge Transfer at the Interface in the Hybrid Photosynthesis System

To gain additional insights into the mechanisms involved in the photocatalytic activity of the autotrophic hybrid photosynthesis systems described here, the photogenerated charge transfer process was evaluated via electrochemical impedance spectroscopy (EIS) (Figure 7). In Nyquist plots obtained from EIS study the semicircle at high frequency is related to the electron transfer-limiting process and its radius corresponds to the charge transfer resistance (Fu et al., 2019; Liu et al., 2020; Han et al., 2018). Thus, a Nyquist plot with a smaller radius indicates lower charge transfer impedance. Here, EIS under light showed that semicircles for g-C_3N_4-catalase (5,000 U mL^{-1}) with *R. eutropha* and pure g-C_3N_4 with *R. eutropha* had smaller radiuses compared with *R. eutropha* alone and *R. eutropha* with catalase, indicating that adding g-C_3N_4 to the bacterial culture lowered the charge transfer impedance and promoted interfacial charge transfer. When catalase was added to either pure g-C_3N_4 or g-C_3N_4 with *R. eutropha*, both Nyquist plots exhibited the smallest semicircle radiuses, which demonstrated that combining g-C_3N_4 with catalase can effectively lower charge transfer resistance and facilitate photogenerated charge transfer at the interface, thus improving H_2 or PHB generation. This is in accordance with the observation that the catalase prevents H_2O_2 poisoning at the surface of g-C_3N_4 and thus promotes charger transfer for proton reduction.

DISCUSSION

The discovery that H_2O_2-degrading enzymes present in the spent medium of *R. eutropha* complete the reaction series required for light-driven water splitting by g-C_3N_4 opens up possibilities for the development of efficient enzymatic PC systems for H_2 production. This new avenue for PC development began to be explored here with the coupling of bovine liver catalase with g-C_3N_4. Although the STH efficiency reported here is promising, it is below 5%–10%, which is considered to be the baseline for economically viable production of H_2 via PC (Chen et al., 2017; Pinaud et al., 2013). It is likely that the water-splitting performance of g-C_3N_4-H_2O_2-degrading enzyme PC can be further improved. Pure g-C_3N_4 has other drawbacks besides H_2O_2 poisoning for optimal photocatalytic activity such as narrow light absorption range below 470 nm, slow surface kinetics, and charge carrier transport as well as important activation energy requirement (Zhang et al., 2017a). Several studies described approaches relying on earth-abundant co-catalysts and on new structural designs to overcome these limitations (Zhang et al., 2017a; Niu et al., 2014). Other groups have improved the photocatalytic activity of g-C_3N_4 by fine-tuning its morphology, by increasing its crystallinity, or by optimizing its chemical arrangement and electronic properties (Lin et al., 2019; Li et al., 2019; Zhang et al., 2017b; Wu et al., 2019; Niu et al., 2012; Guo et al., 2016). Similar strategies could be employed to improve g-C_3N_4-catalase PC. In addition, other catalases or different H_2O_2-degrading enzymes such as peroxidases could be better suited for interacting with g-C_3N_4.

In its lower-cost configuration design, the g-C_3N_4-H_2O_2-degrading enzyme system can split water by coupling g-C_3N_4 with waste medium from microbial cultures. This strategy could create value and store energy under the form of H_2 by harnessing enzyme-rich wastes from bio-industrial processes. For this purpose, water-splitting performance of g-C_3N_4 coupled with biotechnological wastes from different sources containing unique profiles of H_2O_2-degrading enzymes should also be evaluated.

When immersed in an *R. eutropha* culture, g-C_3N_4 splits water and converts light energy into reducing equivalents, which are transferred to bacteria for PHB production. The addition of catalase to this hybrid photosynthesis system significantly improves autotrophic and heterotrophic productivity by curbing H_2O_2 poisoning of g-C_3N_4 and by accelerating water splitting. Simultaneously with H_2O_2 conversion into H_2O and O_2, the catalase may improve photocatalysis by g-C_3N_4 by other means. For instance, it has recently been shown that CDots enable water splitting by g-C_3N_4 and accelerate H_2 production by serving as a catalyst for H_2O_2 decomposition and at the same time as a co-catalyst for H_2 evolution (Qu et al., 2018). Further investigation is required to achieve a complete understanding of the functional interactions between g-C_3N_4 and the catalase enzyme.

The results presented here also show that coupling g-C_3N_4 with a bacterial catalyst significantly expands the photocatalytic products of the abiotic PC beyond H_2 including the conversion of CO_2 into carbon-chain polymers. However, to outcompete autotrophic bioproduction relying on natural photosynthesis, microbial CO_2 reduction driven by g-C_3N_4-catalase needs further improvement. Besides upgrading g-C_3N_4-catalase PC, this can be achieved by optimizing the metabolism of the microbial catalyst and by finding the best compromise in terms of growth conditions and bioreactor configuration to maximize microbial cell and PC activities.

In both the autotrophic and heterotrophic modes, g-C_3N_4-catalase doubled or nearly doubled PHB production by *R. eutropha*, which suggests great potential for CO_2 reduction by hybrid photosynthesis as well as for photoaugmentation of white biotechnologies designed for the conversion of organic substrate into valuable chemicals. In conclusion, the results demonstrate that g-C_3N_4 can harness the activity of H_2O_2-degrading enzymes such as the catalase to split water efficiently under sunlight and generate reducing equivalents for microbial production processes.

Limitations of the Study

A comprehensive study of the mechanisms involved in the transfer of electrons from g-C_3N_4 to *R. eutropha* is necessary to have a complete understanding of the hybrid photosynthesis system described here and be able to improve its performance in the future. A major optimization effort is also needed for practical applications.

METHODS

All methods can be found in the accompanying Transparent Methods supplemental file.

SUPPLEMENTAL INFORMATION

Supplemental Information can be found online at https://doi.org/10.1016/j.isci.2019.100784.

ACKNOWLEDGMENTS

This work was supported by the Chinese Thousand Talents Plan Program and Wuhan University of Technology.

AUTHOR CONTRIBUTIONS

P.-L.T. and T.Z. conceived the study. M.X. carried out the enzymatic photocatalyst experiments and the hybrid photosynthesis experiments. P.-L.T. completed H_2O_2-degrading enzyme activity assay. Y.C. carried out scanning electron microscopy experiments. P.-L.T., M.X., and T.Z. interpreted the data and wrote the manuscript. All the authors reviewed and approved the final manuscript.

DECLARATION OF INTERESTS

The authors declare no competing interests.

Received: August 20, 2019
Revised: November 22, 2019
Accepted: December 12, 2019
Published: January 24, 2020

REFERENCES

Bi, C., Su, P., Müller, J., Yeh, Y.-C., Chhabra, S.R., Beller, H.R., Singer, S.W., and Hillson, N.J. (2013). Development of a broad-host synthetic biology toolbox for *Ralstonia eutropha* and its application to engineering hydrocarbon biofuel production. Microb. Cell Fact. *12*, 107.

Brigham, C.J., Gai, C.S., Lu, J., Speth, D.R., Worden, R.M., and Sinskey, A.J. (2013). Engineering *Ralstonia eutropha* for production of isobutanol from CO_2, H_2, and O_2. In Advanced Biofuels and Bioproducts, J.W. Lee, ed. (Springer New York), pp. 1065–1090.

Chakravarty, J., and Brigham, C.J. (2018). Solvent production by engineered *Ralstonia eutropha*: channeling carbon to biofuel. Appl. Microbiol. Biotechnol. *102*, 5021–5031.

Chen, S., Takata, T., and Domen, K. (2017). Particulate photocatalysts for overall water splitting. Nat. Rev. Mater. *2*, 17050.

Claassens, N.J., Sousa, D.Z., dos Santos, V.A.P.M., de Vos, W.M., and van der Oost, J. (2016). Harnessing the power of microbial autotrophy. Nat. Rev. Microbiol. *14*, 692–706.

Fang, X., Gao, R., Yang, Y., and Yan, D. (2019). A cocrystal precursor strategy for carbon-rich graphitic carbon nitride toward high-efficiency photocatalytic overall water splitting. iScience *16*, 22–30.

Fu, J., Xu, Q., Low, J., Jiang, C., and Yu, J. (2019). Ultrathin 2D/2D WO_3/g-C_3N_4 step-scheme H_2-production photocatalyst. Appl. Catal. B *243*, 556–565.

Grousseau, E., Lu, J., Gorret, N., Guillouet, S.E., and Sinskey, A.J. (2014). Isopropanol production with engineered *Cupriavidus necator* as bioproduction platform. Appl. Microbiol. Biotechnol. *98*, 4277–4290.

Guo, Y., Li, J., Yuan, Y., Li, L., Zhang, M., Zhou, C., and Lin, Z. (2016). A Rapid microwave-assisted thermolysis route to highly crystalline carbon nitrides for efficient hydrogen generation. Angew. Chem. Int. Ed. *55*, 14693–14697.

Guo, J., Suástegui, M., Sakimoto, K.K., Moody, V.M., Xiao, G., Nocera, D.G., and Joshi, N.S. (2018). Light-driven fine chemical production in yeast biohybrids. Science *362*, 813–816.

Han, C., Meng, P., Waclawik, E.R., Zhang, C., Li, X.-H., Yang, H., Antonietti, M., and Xu, J. (2018). Palladium/graphitic carbon nitride (g-C_3N_4) stabilized emulsion microreactor as a store for hydrogen from ammonia borane for use in alkene hydrogenation. Angew. Chem. Int. Ed. *57*, 14857–14861.

Hu, X., Ji, H., Chang, F., and Luo, Y. (2014). Simultaneous photocatalytic Cr(VI) reduction and 2,4,6-TCP oxidation over g-C_3N_4 under visible light irradiation. Catal. Today *224*, 34–40.

Johnson, L.A., and Hug, L.A. (2019). Distribution of reactive oxygen species defense mechanisms across domain bacteria. Free Radic. Biol. Med. *140*, 93–102.

Li, H., Opgenorth, P.H., Wernick, D.G., Rogers, S., Wu, T.-Y., Higashide, W., Malati, P., Huo, Y.-X., Cho, K.M., and Liao, J.C. (2012). Integrated electromicrobial conversion of CO_2 to higher alcohols. Science *335*, 1596.

Li, J., Wu, D., Iocozzia, J., Du, H., Liu, X., Yuan, Y., Zhou, W., Li, Z., Xue, Z., and Lin, Z. (2019). Achieving efficient incorporation of π-electrons into graphitic carbon nitride for markedly improved hydrogen generation. Angew. Chem. Int. Ed. *58*, 1985–1989.

Lin, L., Yu, Z., and Wang, X. (2019). Crystalline carbon nitride semiconductors for photocatalytic water splitting. Angew. Chem. Int. Ed. *58*, 6164–6175.

Liu, J., Zhang, Y., Lu, L., Wu, G., and Chen, W. (2012). Self-regenerated solar-driven photocatalytic water-splitting by urea derived graphitic carbon nitride with platinum nanoparticles. Chem. Commun. *48*, 8826–8828.

Liu, J., Liu, Y., Liu, N., Han, Y., Zhang, X., Huang, H., Lifshitz, Y., Lee, S.-T., Zhong, J., and Kang, Z. (2015a). Metal-free efficient photocatalyst for stable visible water splitting via a two-electron pathway. Science *347*, 970–974.

Liu, C., Gallagher, J.J., Sakimoto, K.K., Nichols, E.M., Chang, C.J., Chang, M.C.Y., and Yang, P. (2015b). Nanowire–bacteria hybrids for unassisted solar carbon dioxide fixation to value-added chemicals. Nano Lett. *15*, 3634–3639.

Liu, C., Colón, B.C., Ziesack, M., Silver, P.A., and Nocera, D.G. (2016). Water splitting–biosynthetic system with CO_2 reduction efficiencies exceeding photosynthesis. Science *352*, 1210–1213.

Liu, Y., He, M., Guo, R., Fang, Z., Kang, S., Ma, Z., Dong, M., Wang, W., and Cui, L. (2020). Ultrastable metal-free near-infrared-driven photocatalysts for H_2 production based on protonated 2D g-C_3N_4 sensitized with chlorin e6. Appl. Catal. B *260*, 118137.

Lu, J., Brigham, C.J., Gai, C.S., and Sinskey, A.J. (2012). Studies on the production of branched-chain alcohols in engineered *Ralstonia eutropha*. Appl. Microbiol. Biotechnol. *96*, 283–297.

Mishra, S., and Imlay, J. (2012). Why do bacteria use so many enzymes to scavenge hydrogen peroxide? Arch. Biochem. Biophys. *525*, 145–160.

Mishra, A., Basu, S., Shetti, N.P., Reddy, K.R., and Aminabhavi, T.M. (2019a). Chapter 27-Photocatalysis of graphene and carbon nitride-based functional carbon quantum dots. In Nanoscale Materials in Water Purification Micro and Nano Technologies, S. Thomas, D. Pasquini, S.-Y. Leu, and D.A. Gopakumar, eds. (Elsevier), pp. 759–781.

Mishra, A., Mehta, A., Basu, S., Shetti, N.P., Reddy, K.R., and Aminabhavi, T.M. (2019b). Graphitic carbon nitride (g–C_3N_4)–based metal-free photocatalysts for water splitting: a review. Carbon *149*, 693–721.

Müller, J., MacEachran, D., Burd, H., Sathitsuksanoh, N., Bi, C., Yeh, Y.-C., Lee, T.S., Hillson, N.J., Chhabra, S.R., Singer, S.W., et al. (2013). Engineering of *Ralstonia eutropha* H16 for autotrophic and heterotrophic production of methyl ketones. Appl. Environ. Microbiol. *79*, 4433–4439.

Nichols, E.M., Gallagher, J.J., Liu, C., Su, Y., Resasco, J., Yu, Y., Sun, Y., Yang, P., Chang, M.C.Y., and Chang, C.J. (2015). Hybrid bioinorganic approach to solar-to-chemical conversion. Proc. Natl. Acad. Sci. USA *112*, 11461–11466.

Niu, P., Zhang, L., Liu, G., and Cheng, H.-M. (2012). Graphene-like carbon nitride nanosheets for improved photocatalytic activities. Adv. Funct. Mater. *22*, 4763–4770.

Niu, P., Yin, L.-C., Yang, Y.-Q., Liu, G., and Cheng, H.-M. (2014). Increasing the visible light absorption of graphitic carbon nitride (melon) photocatalysts by homogeneous self-modification with nitrogen vacancies. Adv. Mater. *26*, 8046–8052.

Pinaud, B.A., Benck, J.D., Seitz, L.C., Forman, A.J., Chen, Z., Deutsch, T.G., James, B.D., Baum, K.N., Baum, G.N., Ardo, S., et al. (2013). Technical and economic feasibility of centralized facilities for solar hydrogen production via photocatalysis and photoelectrochemistry. Energy Environ. Sci. *6*, 1983–2002.

Pohlmann, A., Fricke, W.F., Reinecke, F., Kusian, B., Liesegang, H., Cramm, R., Eitinger, T., Ewering, C., Pötter, M., Schwartz, E., et al. (2006). Genome sequence of the bioplastic-producing "Knallgas" bacterium *Ralstonia eutropha* H16. Nat. Biotechnol. *24*, 1257–1262.

Prévot, M.S., and Sivula, K. (2013). Photoelectrochemical tandem cells for solar water splitting. J. Phys. Chem. C *117*, 17879–17893.

Qu, D., Liu, J., Miao, X., Han, M., Zhang, H., Cui, Z., Sun, S., Kang, Z., Fan, H., and Sun, Z. (2018). Peering into water splitting mechanism of g-C_3N_4-carbon dots metal-free photocatalyst. Appl. Catal. B *227*, 418–424.

Rao, V.N., Reddy, N.L., Kumari, M.M., Cheralathan, K.K., Ravi, P., Sathish, M., Neppolian, B., Reddy, K.R., Shetti, N.P., Prathap, P., et al. (2019). Sustainable hydrogen production for the greener environment by quantum dots-based efficient photocatalysts: a review. J. Environ. Manage. *248*, 109246.

Reddy, K.R., Reddy, C.H.V., Nadagouda, M.N., Shetti, N.P., Jaesool, S., and Aminabhavi, T.M. (2019). Polymeric graphitic carbon nitride (g-C_3N_4)-based semiconducting nanostructured materials: synthesis methods, properties and photocatalytic applications. J. Environ. Manage. *238*, 25–40.

Sakimoto, K.K., Wong, A.B., and Yang, P. (2016a). Self-photosensitization of nonphotosynthetic bacteria for solar-to-chemical production. Science *351*, 74–77.

Sakimoto, K.K., Zhang, S.J., and Yang, P. (2016b). Cysteine–cystine photoregeneration for oxygenic photosynthesis of acetic acid from CO_2 by a tandem inorganic–biological hybrid system. Nano Lett. *16*, 5883–5887.

Tanaka, K., Ishizaki, A., Kanamaru, T., and Kawano, T. (1995). Production of poly(D-3-hydroxybutyrate) from CO_2, H_2, and O_2 by high cell density autotrophic cultivation of *Alcaligenes eutrophus*. Biotechnol. Bioeng. *45*, 268–275.

Tremblay, P.-L., Angenent, L.T., and Zhang, T. (2017). Extracellular electron uptake: among autotrophs and mediated by surfaces. Trends Biotechnol. *35*, 360–371.

Volodina, E., Raberg, M., and Steinbüchel, A. (2016). Engineering the heterotrophic carbon sources utilization range of *Ralstonia eutropha* H16 for applications in biotechnology. Crit. Rev. Biotechnol. *36*, 978–991.

Wang, X., Maeda, K., Thomas, A., Takanabe, K., Xin, G., Carlsson, J.M., Domen, K., and Antonietti, M. (2009). A metal-free polymeric photocatalyst for hydrogen production from water under visible light. Nat. Mater. *8*, 76–80.

Wang, M., Shen, S., Li, L., Tang, Z., and Yang, J. (2017). Effects of sacrificial reagents on photocatalytic hydrogen evolution over different photocatalysts. J. Mater. Sci. *52*, 5155–5164.

Wu, D., Hu, S., Xue, H., Hou, X., Du, H., Xu, G., and Yuan, Y. (2019). Protonation and microwave-assisted heating induced excitation of lone-pair electrons in graphitic carbon nitride for increased photocatalytic hydrogen generation. J. Mater. Chem. A *7*, 20223–20228.

Xu, M., Tremblay, P.-L., Jiang, L., and Zhang, T. (2019). Stimulating bioplastic production with light energy by coupling *Ralstonia eutropha* with the photocatalyst graphitic carbon nitride. Green Chem. *21*, 2392–2400.

Yan, S.C., Lv, S.B., Li, Z.S., and Zou, Z.G. (2010). Organic–inorganic composite photocatalyst of g-C_3N_4 and TaON with improved visible light photocatalytic activities. Dalton Trans. *39*, 1488–1491.

Ye, S., Wang, R., Wu, M.-Z., and Yuan, Y.-P. (2015). A review on g-C_3N_4 for photocatalytic water splitting and CO_2 reduction. Appl. Surf. Sci. *358*, 15–27.

Ye, J., Yu, J., Zhang, Y., Chen, M., Liu, X., Zhou, S., and He, Z. (2019). Light-driven carbon dioxide reduction to methane by *Methanosarcina barkeri*-CdS biohybrid. Appl. Catal. B *257*, 117916.

Zhang, T. (2015). More efficient together. Science *350*, 738–739.

Zhang, Y., Zhang, Q., Shi, Q., Cai, Z., and Yang, Z. (2015). Acid-treated g-C_3N_4 with improved photocatalytic performance in the reduction of aqueous Cr(VI) under visible-light. Sep. Purif. Technol. *142*, 251–257.

Zhang, G., Lan, Z.-A., Lin, L., Lin, S., and Wang, X. (2016). Overall water splitting by Pt/g-C_3N_4 photocatalysts without using sacrificial agents. Chem. Sci. *7*, 3062–3066.

Zhang, T., and Tremblay, P.-L. (2017). Hybrid photosynthesis-powering biocatalysts with solar energy captured by inorganic devices. Biotechnol. Biofuels *10*, 249.

Zhang, G., Lan, Z.-A., and Wang, X. (2017a). Surface engineering of graphitic carbon nitride polymers with cocatalysts for photocatalytic overall water splitting. Chem. Sci. *8*, 5261–5274.

Zhang, G., Savateev, A., Zhao, Y., Li, L., and Antonietti, M. (2017b). Advancing the n $\rightarrow \pi^*$ electron transition of carbon nitride nanotubes for H_2 photosynthesis. J. Mater. Chem. A *5*, 12723–12728.

Zhang, H., Liu, H., Tian, Z., Lu, D., Yu, Y., Cestellos-Blanco, S., Sakimoto, K.K., and Yang, P. (2018). Bacteria photosensitized by intracellular gold nanoclusters for solar fuel production. Nat. Nanotechnol. *13*, 900.

iScience, Volume *23*

Supplemental Information

Nonmetallic Abiotic-Biological Hybrid Photocatalyst for Visible Water Splitting and Carbon Dioxide Reduction

Pier-Luc Tremblay, Mengying Xu, Yiming Chen, and Tian Zhang

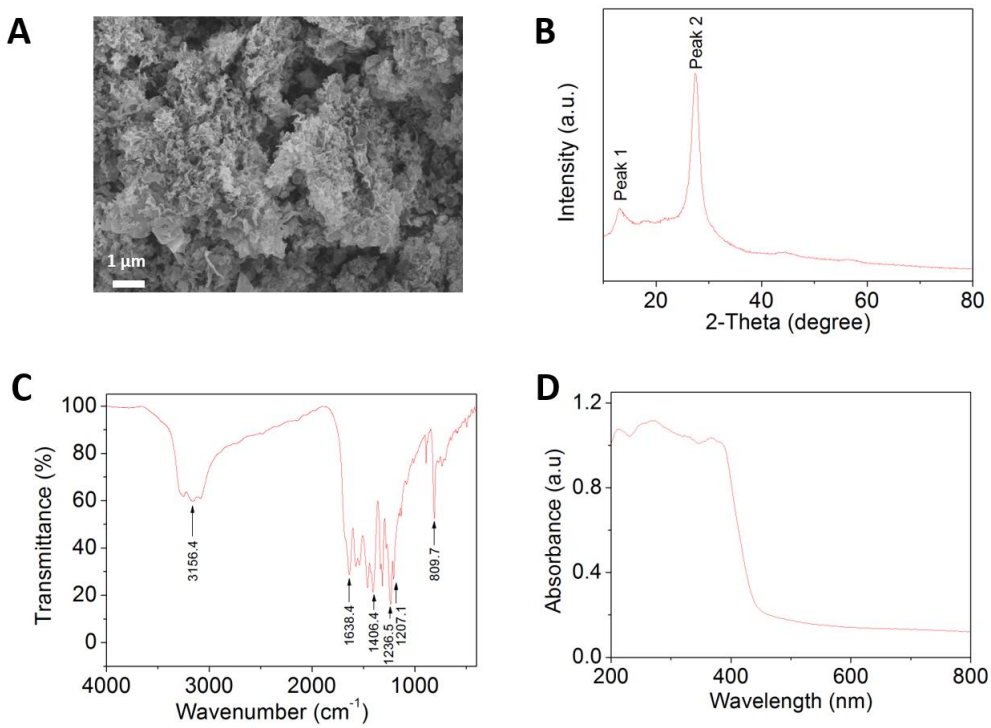

Figure S1. g-C_3N_4 characterization. (A) SEM image, **(B)** XRD, **(C)** FT-IR, and **(D)** UV-visible diffuse reflectance spectra of synthesized g-C_3N_4. X-ray diffraction (XRD) shows the two main characteristic peaks associated with g-C_3N_4. The first peak at 13.2° corresponds to tri-s-triazine units packing in the lattice planes parallel to the c axis. The second peak at 27.6° is attributed to the interlayer stacking of aromatic segments (Mao et al., 2017; Zang et al., 2014; Cheng et al., 2016). The Fourier transform infrared spectrum (FT-IR) includes skeletal vibrations in the range of 1200-1650 cm^{-1} for aromatic C-N heterocycles and a breathing vibration at 809.7 cm^{-1} for tri-s-triazine units characteristic of g-C_3N_4. Between 3000-3500 cm^{-1}, a broad absorption peak is observed corresponding to stretching vibrational modes of the O-H or N-H groups (Tang et al., 2015; Wang et al., 2017). The UV-visible light absorption spectrum is also typical of g-C_3N_4 with an upper limit at *ca.* 450 nm (Patnaik et al., 2017). Related to Figures 1, 2, and 3.

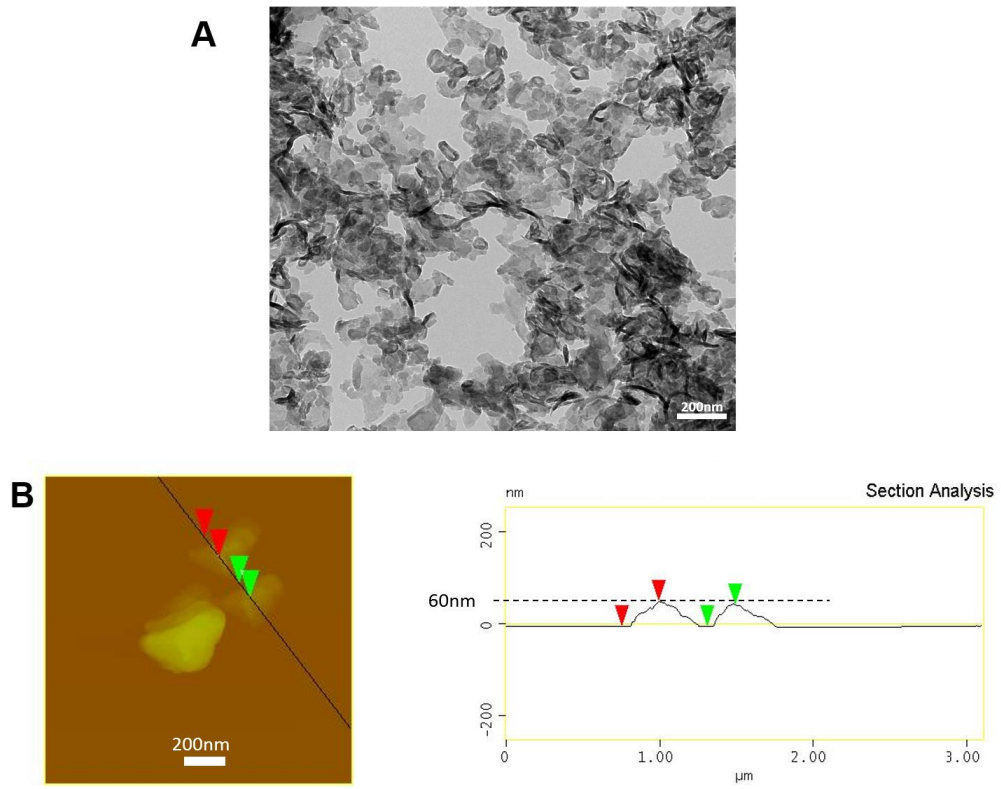

Figure S2. TEM and AFM analysis of g-C_3N_4 particles. (A) TEM image shows typical layered sheet-like structure of g-C_3N_4.[7] **(B)** Section analysis of the AFM image shows that the thickness of the g-C_3N_4 sheet-like particles was ca. 60 nm. Related to Figures 1, 2, and 3.

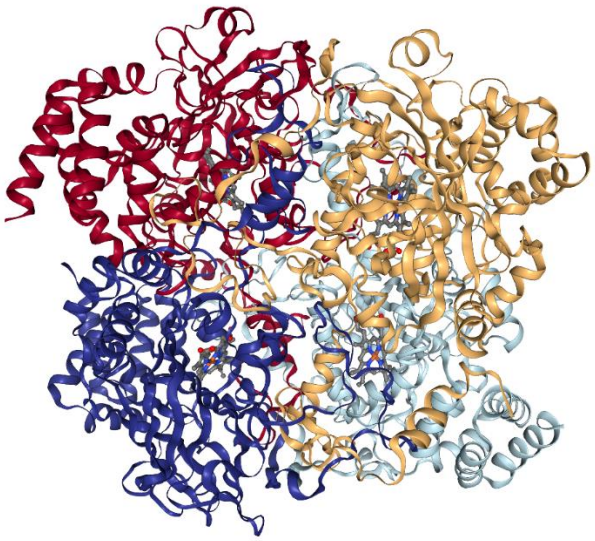

Figure S3. The crystal structure of the bovine liver catalase. The enzyme comprises four 60 kDa subunits. Each of these subunits contains an iron bound to a protoheme IX group (PDB ID: 1TGU; Sugadev, R., Balasundaresan, D., Ponnuswamy, M.N., Kumaran, D., Swaminathan, S., Sekar, K. The crystal structure of bovine liver catalase.). One unit of bovine liver catalase will degrade 1.0 μmole H_2O_2 min^{-1} at pH 7.0 at 25 °C according to the reaction $2H_2O_2 \rightarrow 2H_2O + O_2$. Related to Figures 3 and 4.

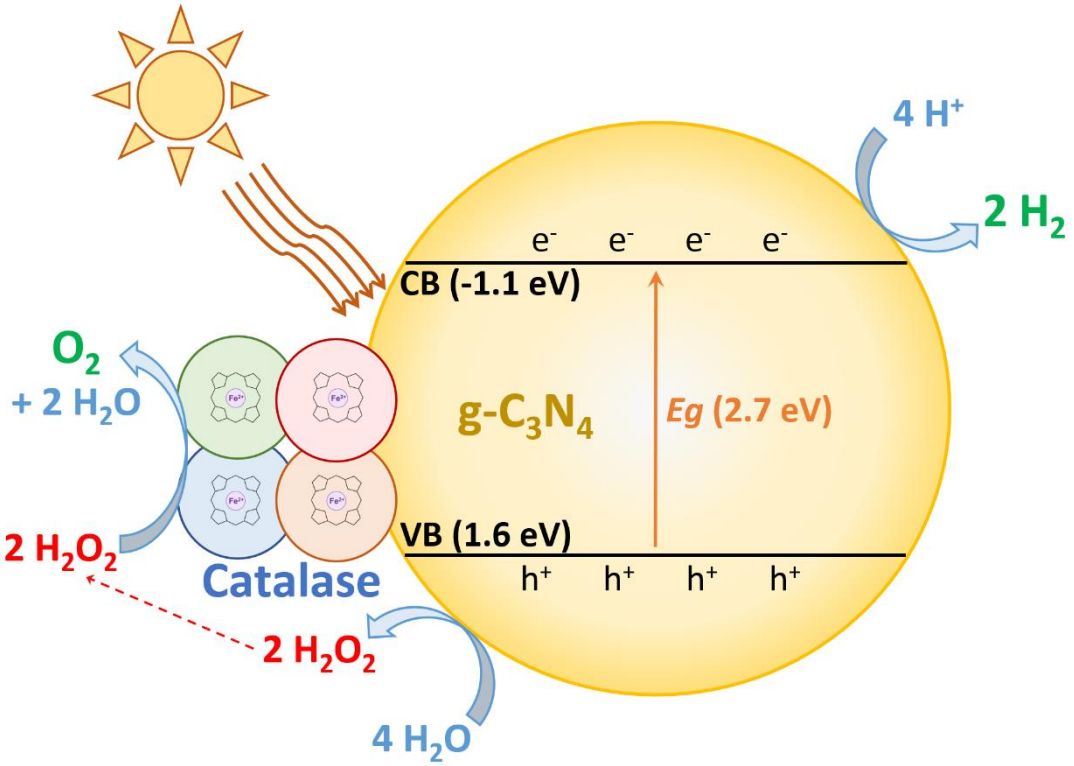

Figure S4. Schematic diagram of the g-C_3N_4-catalase enzymatic photocatalyst system. Water is oxidized to H_2O_2 by g-C_3N_4 under light. The bovine liver catalase decomposes H_2O_2 into O_2 and H_2O preventing H_2O_2 poisoning of g-C_3N_4. Concomitantly, protons are converted into H_2 by g-C_3N_4, thus completing the light-driven water-splitting reaction. CB: conduction band. VB: valence band. Related to Figures 3 and 4.

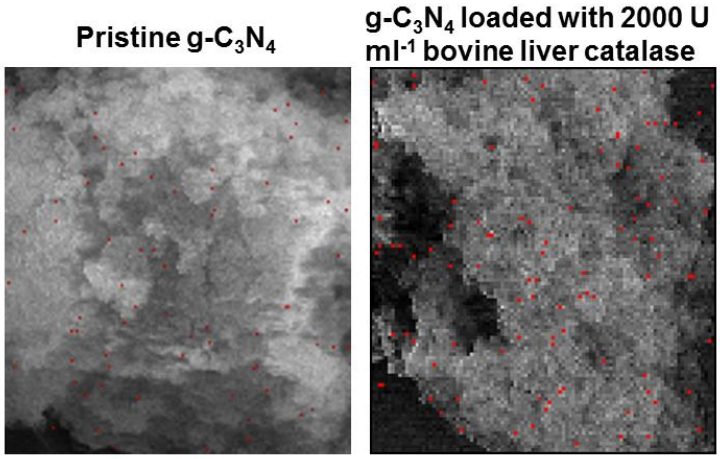

	Weight percentage	
Element	**Pristine g-C_3N_4**	**g-C_3N_4 with catalase**
Fe	0.18	1.74
C	38.90	40.22
N	60.93	58.04

Figure S5. SEM images of pristine g-C_3N_4 and g-C_3N_4 loaded with 2000 U mL^{-1} bovine liver catalase with iron elemental mapping and weight percentage for carbon, nitrogen, and iron. Elemental mapping and weight percentage were examined by energy dispersive X-Ray spectroscopy (EDS). Red dots on SEM images correspond to iron elements. Iron elements are bound to the four protoheme IX groups attached to the bovine liver catalase. Increased iron element weight percentage indicates the presence of catalase in the vicinity of g-C_3N_4. Related to Figures 3 and 4.

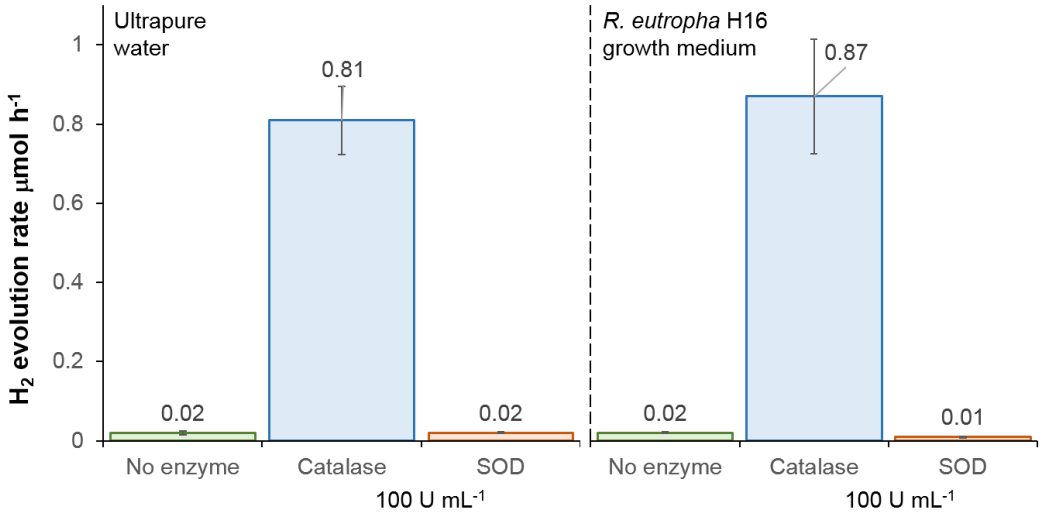

Figure S6. Light-driven water-splitting activity of g-C_3N_4 with catalase or SOD. Impact of 100 U mL^{-1} bovine liver catalase or SOD on H_2 evolution rate by g-C_3N_4 suspended in ultrapure water or *R. eutropha* growth medium under 4200 lux LED light. Each bar is the average of at least three replicates with standard deviation. Related to Figures 3 and 4.

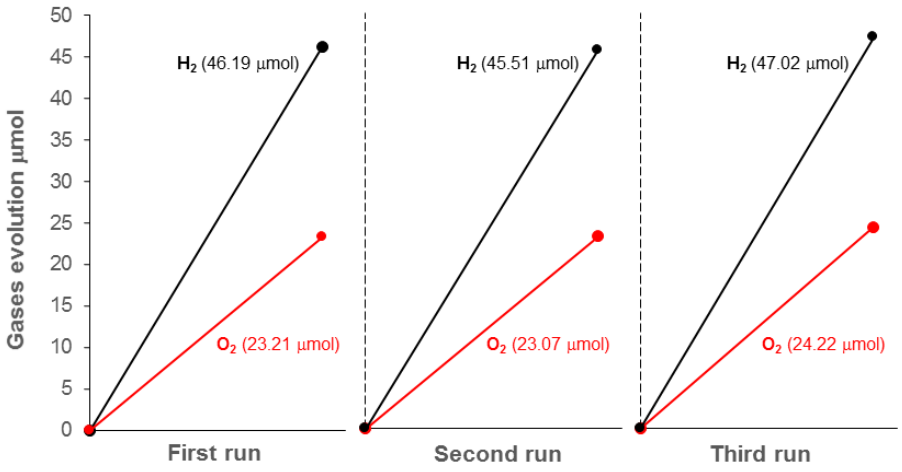

Figure S7. Cycling test for the g-C_3N_4-catalase PC system. H_2 and O_2 evolution by g-C3N4 with 10000 U mL^{-1} catalase under a light intensity of 200 W m^{-2} was monitored for several cycles of one hour. Related to Figures 3 and 4.

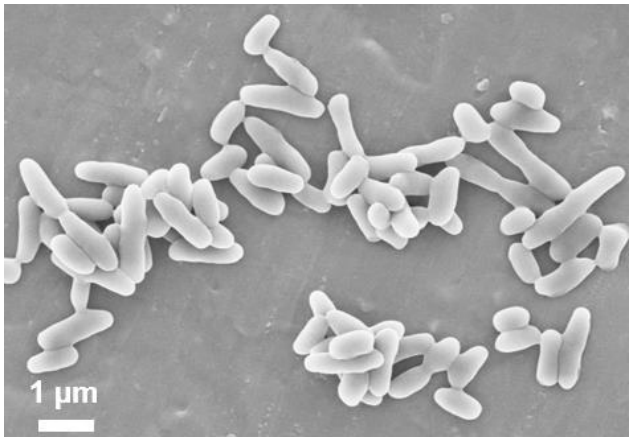

Figure S8. SEM image of *R. eutropha* H16 cells without g-C_3N_4. *R. eutropha* H16 is a Gram-negative rod-shape bacterium of the *Burkholderiaceae* family. *R. eutropha* H16 is also named *Cupriavidus necator* H16. Related to Figures 5 and 6.

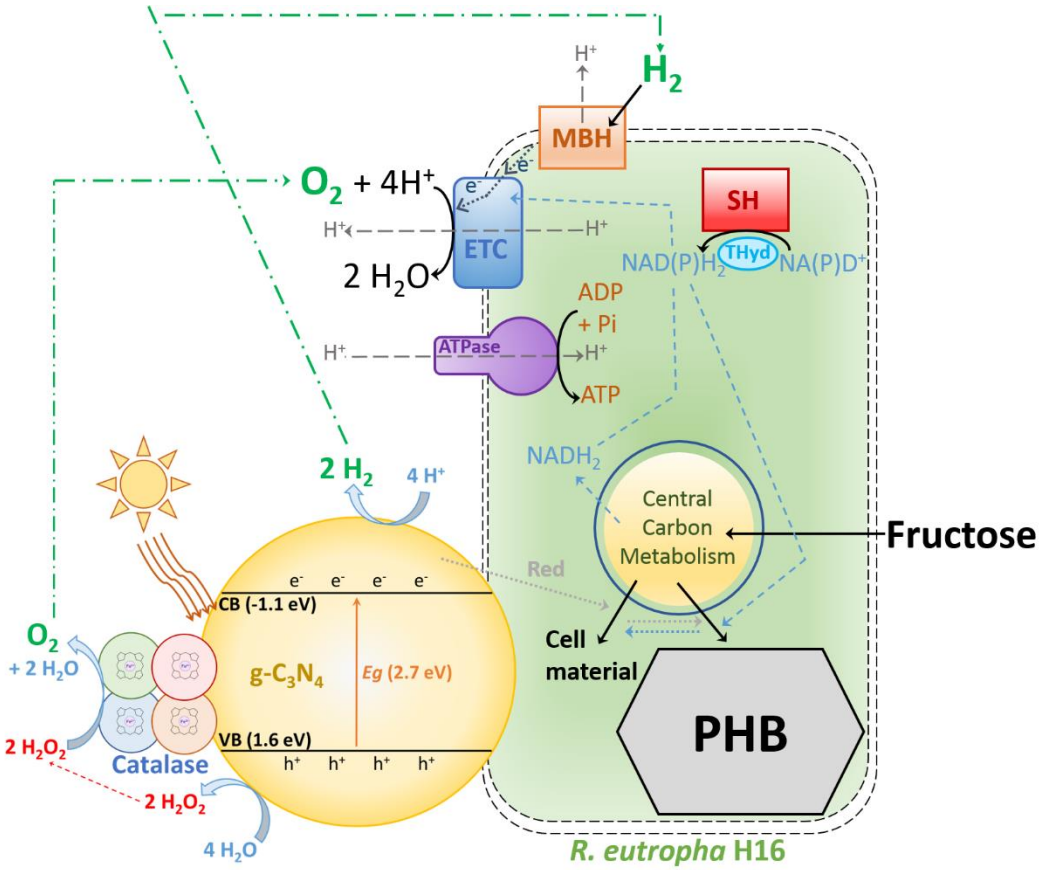

Figure S9. Schematic diagram of heterotrophic hybrid photosynthesis with g-C_3N_4-catalase and *R. eutropha* producing PHB from fructose. Water-splitting g-C_3N_4-catalase augments heterotrophic PHB production either by providing H_2 and/or O_2 molecules for the bacterial metabolism or by transferring unknown reducing equivalents (Red) to *R. eutropha*. ETC: electron transport chain. MBH: membrane-bound hydrogenase. SH: soluble hydrogenase. Thyd: $NAD(P)^+$ transhydrogenase. Related to Figure 6.

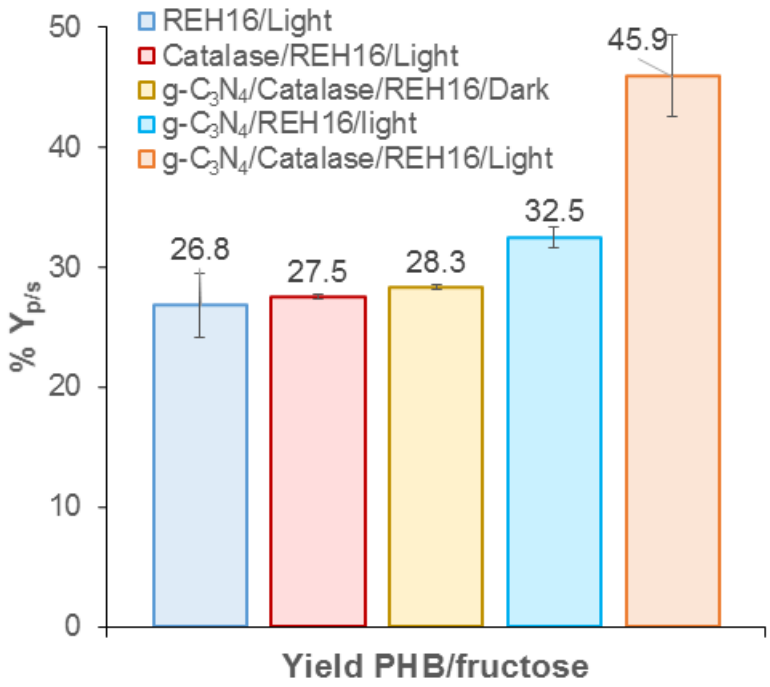

Figure S10. Impact of water-splitting g-C_3N_4-catalase on PHB to fructose yield of heterotrophically-grown *R. eutropha*. Yield gram PHB produced per gram fructose consumed ($Y_{p/s}$) after 96 hours of growth. REH16: *R. eutropha* H16. Each bar is the mean of at least three replicates with standard deviation. Related to Figure 6.

Table S1. Gene in *R. eutropha* H16 coding for H_2O_2-degrading enzyme catalase and peroxidase.[a]

Gene/locus	Annotation
Catalase	
katE1/H16_A3109	Catalase KatE1
katE2/H16_B1428	Catalase KatE2
katG/H16_A2777	Catalase (peroxidase I) KatG
Peroxidase	
H16_B0946	Predicted iron-dependent peroxidase
tpx/H16_A3175	Thiol peroxidase Tpx
H16_A3102	Glutathione peroxidase
H16_A0065	Glutathione peroxidase
H16_A3267	Peroxiredoxin
H16_A1460	Peroxiredoxin

[a]Related to Figure 2.

Table S2. Metal-free g-C_3N_4-based particulate photocatalyst systems splitting water under visible light.[a]

System	Performance	Comments	Reference
g-C_3N_4 with carbon nanodots	H_2 evolution: 191.7 μmol h^{-1} O_2 evolution: nearly stoichiometric STH[b]:2.0%	-80 mg PC[c] in 150 ml ultrapure water -AM 1.5G solar simulator	Liu et al., 2015
carbon-rich g-C_3N_4	H_2 evolution: 530 μmol h^{-1} g^{-1} catalyst O_2 evolution: nearly stoichiometric STH: Not reported	-30 mg PC in 80 ml distilled water -300 W Xe lamp (≥ 300 nm)	Fang et al., 2019
g-C_3N_4-catalase	H_2 evolution: 55.72 μmol h^{-1} O_2 evolution: nearly stoichiometric STH: 3.40% (200 W m^{-2})[d] and 1.00% (800 W m^{-2})[d]	-30 mg PC in 20 ml CAT buffer[e] -500 W Xe lamp with an AM1.5G filter	This work

[a]Related to Figure 4.

[b]STH: Solar-to-H_2 efficiency.

[c]PC: photocatalyst.

[d]Light intensity.

[e]CAT buffer: 50 mM KH_2PO_4 pH 7.4.

Table S3. Hybrid photosynthesis system with particulate photocatalyst for CO_2 reduction.[a]

Particulate photocatalyst	**Microbe**	**Comments**	**Reference**
CdS nanoparticles	*Moorella thermoacetica*	-Cysteine as sacrificial e^- donor -*Ca.* 1.1 mM acetate produced in 36 hours	Sakimoto et al., 2016a
CdS and TiO_2 nanoparticles	*M. thermoacetica*	-Z-scheme, water splitting -Cysteine as e^- shuttle -cocatalyst MnPc -*Ca.* 0.8 mM acetate produced in one day	Sakimoto et al., 2016b
CdS nanoparticles	*Methanosarcina barkeri*	-Cysteine as sacrificial e^- donor - 0.19 μmol h^{-1} methane	Ye et al., 2019
CdS nanoparticles	*Rhodopseudomonas palustris*	-Cysteine as sacrificial e^- donor -Biomass, carotenoids and polyhydroxybutyrate (PHB) production was increased to 148%, 122%, and 147%	Wang et al., 2019
g-C_3N_4	*Ralstonia eutropha* H16	-Water splitting -1.5-fold increase of PHB production	This work
g-C_3N_4 with catalase	*R. eutropha* H16	-Water splitting -2.2-fold increase of PHB production	This work

[a]Related to Figure 5.

TRANSPARENT METHODS

g-C_3N_4 preparation

g-C_3N_4 particles were prepared by a facile thermal treatment of urea as described previously (Liu et al., 2011). 10 g urea was placed into a semi-closed quartz crucible and then calcined in a muffle furnace for two hours with a heating rate of 10 °C min^{-1} up to 550 °C. The bulk product was filtered and washed three times with 20 mL 0.1 M HNO_3 and then washed five times with 20 mL ultrapure water to remove impurities from the sample surface. g-C_3N_4 was then dried at 55 °C for 24 h and ground into powder.

g-C_3N_4 characterization

The characterization of g-C_3N_4 was done with X-ray powder diffraction (XRD), Fourier-transform infrared spectroscopy (FT-IR), and UV-visible diffuse reflectance spectroscopy. The XRD spectrum of g-C_3N_4 was recorded within the scan range of 2θ from 10^0 to 80^0 using a D8 ADVANCE powder X-ray diffractometer (Bruker, MA, USA) equipped with Cu Kα X-ray. The FT-IR spectrum of g-C_3N_4 was obtained with a Nicolet iS5 FT-IR spectrometer (Thermo Fisher Scientific, MA, USA) using the KBr pellet method within the 400–4000 cm^{-1} range at a 0.8 cm^{-1} resolution. The UV-Visible diffuse reflectance absorption spectrum of the photocatalyst (PC) was recorded with a Lambda 750s spectrophotometer (PerkinElmer, MA, USA).

Bacterial strain and growth medium

The bacterium *R. eutropha* H16 (DSM-428) was used for this study. All bacterial cultures were grown at 30 ^{0}C in a nitrogen-limiting minimal medium, which has a pH of 6.8 (Budde et al., 2010). Components of the minimal medium per liter of ultrapure water are: 1 mL L^{-1} trace mineral mix, 1 g L^{-1} NH_4Cl, 5.2 g L^{-1} $NaH_2PO_4 \cdot 2H_2O$, 11.6 g L^{-1} $Na_2HPO_4 \cdot 12H_2O$, 0.45 g L^{-1} K_2SO_4, 0.8 g L^{-1} $MgSO_4 \cdot 7H_2O$, and 0.08 g L^{-1} $CaCl_2 \cdot 2H_2O$. Components of the trace mineral mix per liter of 0.1 M HCl are: 15 g L^{-1} $FeSO_4 \cdot 7H_2O$, 2.4 g L^{-1} $MnSO_4 \cdot H_2O$, 2.4 g L^{-1} $ZnSO_4 \cdot 7H_2O$, and 0.48 g L^{-1} $CuSO_4 \cdot 5H_2O$.

Under heterotrophic conditions, *R. eutropha* was grown in flasks containing 50 mL minimal medium with 20 g L^{-1} fructose. Under autotrophic conditions, *R. eutropha* H16 was grown in rubber stopper-sealed serum bottles containing 100 mL fructose-free minimal medium under a N_2:H_2:O_2:CO_2 (49:37:7:7) atmosphere.

Cell-free spent medium preparation, pronase treatment, H_2O_2-degrading enzymatic activity, and total protein concentration

For cell-free spent medium preparation, a *R. eutropha* culture grown with fructose for 40 hours was centrifuged at 10000 x g for 10 minutes at 4 ^{0}C. The supernatant was collected and centrifuged for a second time to ensure the complete removal of *R. eutropha* cells. The supernatant from the second centrifugation was considered as cell-free spent medium. For protein degradation treatment, 1 mg mL^{-1} pronase was added to

the cell-free spent medium, which was then incubated overnight at 37 ^{0}C. Total protein concentration in cell-free spent medium was measured with the M5 BCA protein assay kit (Mei5 Biotechnology, China).

H_2O_2-degrading enzymatic activity was measured as described before with several modifications (Beers and Sizer, 1952). 10 mM H_2O_2 was added into sterile minimal medium or cell-free spent medium pre-incubated at 30 ^{0}C. 400 μL of the reaction was quickly transferred to a quartz cuvette and absorbance at 240 nm was monitored over time with an Evolution 220 UV-Visible spectrophotometer (Thermo Fisher Scientific, USA). H_2O_2 concentration was calculated according to equation (1).

$$A = \varepsilon cl \qquad (1)$$

Where A is the absorbance, c is the concentration, l is the light path length (1 cm), and ε is the molar extinction coefficient, which is 43.6 M^{-1} cm^{-1} for H_2O_2 at a wavelength of 240 nm.

Photocatalytic H_2, O_2, and H_2O_2 evolution under a 4200 lux LED light

The photocatalytic evolution experiments of H_2, O_2, and H_2O_2 were carried out in rubber stopper-sealed 120 mL serum bottles incubated at 30 ^{0}C into a CZL-P280D LED light incubator (Hua De Li, China) set at 4200 lux. Serum bottles contained 10 mg g-C_3N_4 particles dispersed in 20 mL ultrapure water, 50 mM KH_2PO_4 buffer pH 7.4

(CAT), sterile minimal medium, or cell-free spent medium. Where indicated, 10, 100, 500, or 2000 U mL^{-1} bovine liver catalase (Yuan Ye, China) or 100 U mL^{-1} superoxide dismutase (Yuan Ye) was added to the PC suspension. Prior to photocatalytic experiments, g-C_3N_4 suspensions were flushed with pure nitrogen for 20 minutes. Where indicated, 5% (w/v) triethanolamine (TEOA) was added to the PC suspension.

H_2 and O_2 were measured with a GC9720 Plus gas chromatograph (FULI, China) equipped with a 5A molecular sieve column and a thermal conductivity detector (TCD). For H_2O_2 measurement, 1 mL g-C_3N_4 suspension was sampled and centrifuged at 7000 x g for 1 minute. The top 400 µl of the supernatant was transferred to a quartz spectrophotometer cuvette and H_2O_2 concentration was measured at 240 nm.

g-C_3N_4-catalase activity under a solar simulator

The photocatalytic activity of g-C_3N_4 suspended in CAT buffer containing 2000, 5000, or 10000 U mL^{-1} bovine liver catalase was evaluated at room temperature under a PL-XQ 500 W Xe lamp (Pu Lin Sai Si, China) equipped with an air mass 1.5 global conditions filter (AM1.5G) with a light intensity of 200 W m^{-2} or 800 W m^{-2} (ca. 0.2 to 0.8 sun). For quantum efficiency (QE_{420nm}) determination, the Xe lamp was instead equipped with a band-pass filter of 420 ± 20 nm. The intensity of the light reaching g-C_3N_4-catalase was measured with a TES-132 light radiometer (TES, China). Nitrogen-flushed serum bottles with g-C_3N_4-catalase were prepared as described above with the exception that 30 mg PC was in suspension instead of 10 mg. For the cycling test, H_2

and O_2 evolution by g-C_3N_4 were measured three times with 10000 U mL^{-1} catalase under a light intensity of 200 W m^{-2}. Between each run, the headspace of the serum bottle was flushed 20 minutes with pure nitrogen.

Solar-to-hydrogen efficiency and quantum efficiency calculations

The solar-to-hydrogen (STH) efficiency was evaluated with the 500 W Xe lamp equipped with an AM1.5G filter according to equation (2).

$$\text{STH \%} = 100E_{H_2} / Es\ A \text{ or } 100\Delta G^0_{H_2} R_{H_2} / Es\ A \qquad (2)$$

Where E_{H_2} is the energy stored in H_2, Es is the light energy radiation per m^2 per second (J m^{-2} s^{-1}), A is the illumination area in m^2, $\Delta G^0_{H_2}$ is the standard Gibbs energy of 237200 J mol^{-1} at 297 K for the energy storage reaction generating H_2, and R_{H_2} is the H_2 evolution rate in mol s^{-1}.

QE_{420nm} was calculated according to equations (3) and (4).

QE_{420nm} % =

2 x number of evolved H_2 molecules / number of incident photons x 100 (3)

$$\text{Number of incident photons} = IAt\lambda / hc \qquad (4)$$

Where I is the light intensity in W m^{-2}, A is the illumination area in m^2, t is the time in second, λ is the wavelength, h is the Planck constant $6.626x10^{-34}$ J s, and c is the speed of light $3x10^8$ m s^{-1}.

Hybrid photosynthesis with *R. eutropha* and g-C_3N_4-catalase

For autotrophic hybrid photosynthesis, *R. eutropha* grown to mid-log with CO_2 as sole carbon source was used as inoculum. A serum bottle containing 100 mL minimal medium with 0.5 g L^{-1} g-C_3N_4 and 5000 U mL^{-1} bovine liver catalase under a N_2:H_2:CO_2:O_2 atmosphere was inoculated with CO_2-grown *R. eutropha* at an initial optical density (OD_{600nm}) of 0.01, and then it was incubated at 30 ^{0}C under LED light at an intensity of 4200 lux. PHB production was monitored during 48 hours. For heterotrophic hybrid photosynthesis, a fructose-grown *R. eutropha* mid-log culture was used to inoculate a flask containing 0.5 g L^{-1} g-C_3N_4 and 5000 U mL^{-1} bovine liver catalase in 50 mL minimal medium with 20 g L^{-1} fructose. The initial OD_{600nm} was 0.05. Both PHB production and fructose consumption were monitored over 96 hours for the heterotrophic g-C_3N_4-catalase-*R. eutropha* system, which was incubated at 30 °C under LED light at an intensity of 4200 lux. Controls without g-C_3N_4, catalase, or light exposure were also tested for PHB production.

PHB, fructose, and production yield

PHB was extracted and measured as described previously (Xu et al., 2019; Braunegg et al., 1978). 10 mL of PHB-containing samples were centrifuged at 7000 x g for 10 minutes at 4 °C. Cell pellets were washed twice with ultrapure water before being dried overnight at 55 °C. Samples were added to 2 mL methanol acidified with 3% (v/v)

H_2SO_4. Extraction mixtures were then incubated for 4 hours in screw-capped glass tubes at 100 ^{0}C. After cooling of the samples at room temperature, 1 mL ultrapure water was added to the extraction mixtures, which were then shaken vigorously for 1 minute. The organic phase was removed after separation from the aqueous phase and transferred to a glass vial. Extracted PHB in the organic phase was measured with a GC9720 gas chromatograph (Fuli) equipped with a RB-FFAP column and a flame ionization detector (FID). The gas chromatograph column was maintained at an initial temperature of 50 °C for 2 minutes with subsequent temperature increase rate of 10 ^{0}C min^{-1} up to 220 ^{0}C for 2 minutes.

Fructose concentration was measured with a Breeze 2 high-performance liquid chromatograph (Waters, MA, USA) equipped with a Refractive Index Detector and an Aminex HPX-87H anion exchange column (Bio-Rad, CA, USA) set at a temperature of 50 °C. The mobile phase was 5 mM H_2SO_4 at a flow rate of 0.6 ml min^{-1}. Yield of PHB production to fructose consumption is calculated according to equation (5).

$Y_{p/s}$ = grams PHB ($[C_4H_6O_2]n$) produced / grams fructose ($C_6H_{12}O_6$) consumed (5)

Microscopy and energy-dispersive X-ray diffraction

The structure of g-C_3N_4 particles was characterized by SEM, TEM, and atomic force microscopy (AFM). Elemental mapping of g-C_3N_4 samples with or without 2000 U mL^{-1} bovine liver catalase was completed by energy dispersive X-ray spectroscopy (EDS).

Both SEM and EDS were performed with a S-4800 Field-emission scanning electron microscope (Hitachi, Japan). Samples were dropped on a silicon wafer and air-dried before being scanned at an accelerating voltage of 5 kV. For TEM, g-C_3N_4 samples were dispersed into ethanol by ultrasonic treatment and diluted before being dropped on a copper grid. TEM images were obtained with a JEM-1400Plus (JEOL, Japan) microscope at an accelerating voltage of 120 kV. AFM analysis was performed with a Nanoscope IV (Veeco, NY).

For SEM of hybrid photosynthesis system, 24-hours autotrophic or heterotrophic bacterial cultures with g-C_3N_4-catalase were collected and fixed overnight at 4 ^{0}C in a 0.1 M Na phosphate buffer (pH 7.0) containing 2.5% glutaraldehyde. Samples were then washed one time serially with 30%, 50%, 70%, 80%, 90% ethanol and two times with 100% ethanol. Samples suspended in 100% ethanol were dropped on a silicon wafer and air-dried, and then they were scanned at an accelerating voltage of 5 kV. The same procedure was employed to prepare the hybrid photosynthesis samples for TEM with the exception that g-C_3N_4-catalase with *R. eutropha* H16 was dropped on a copper grid instead of silicon wafer.

Electrochemical impedance spectroscopy (EIS)

Photoelectrochemical measurements were conducted with a CHI600E potentiostat (CH Instruments, TX, USA) using a three-electrode system with *R. eutropha* autotrophic growth medium as electrolyte. A glassy carbon electrode (diameter of 3 mm) served as

the working electrode, a platinum sheet was used as the counter electrode, and an Ag/AgCl electrode (3.5 M KCl) was employed as the reference electrode. EIS spectra were acquired with a sinusoidal perturbation of 5 mV amplitude and frequencies ranging from 100 kHz to 0.1 Hz at -1.2 V versus Ag/AgCl under illumination.

REFERENCES

Beers, R.F., and Sizer, I.W. (1952). A spectrophotometric method for measuring the breakdown of hydrogen peroxide by catalase. J. Biol. Chem. *195*, 133–140.

Braunegg, G., Sonnleitner, B., and Lafferty, R.M. (1978). A rapid gas chromatographic method for the determination of poly-β-hydroxybutyric acid in microbial biomass. European J. Appl. Microbiol. Biotechnol. *6*, 29–37.

Budde, C.F., Mahan, A.E., Lu, J., Rha, C., and Sinskey, A.J. (2010). Roles of multiple acetoacetyl coenzyme A reductases in polyhydroxybutyrate biosynthesis in *Ralstonia eutropha* H16. J. Bacteriol. *192*, 5319–5328.

Cheng, R., Fan, X., Wang, M., Li, M., Tian, J., and Zhang, L. (2016). Facile construction of $CuFe_2O_4$/g-C_3N_4 photocatalyst for enhanced visible-light hydrogen evolution. RSC Adv. *6*, 18990–18995.

Fang, X., Gao, R., Yang, Y., and Yan, D. (2019). A cocrystal precursor strategy for carbon-rich graphitic carbon nitride toward high-efficiency photocatalytic overall water splitting. iScience *16*, 22–30.

Liu, J., Zhang, T., Wang, Z., Dawson, G., and Chen, W. (2011). Simple pyrolysis of urea into graphitic carbon nitride with recyclable adsorption and photocatalytic activity. J. Mater. Chem. *21*, 14398–14401.

Liu, J., Liu, Y., Liu, N., Han, Y., Zhang, X., Huang, H., Lifshitz, Y., Lee, S.-T., Zhong, J., and Kang, Z. (2015). Metal-free efficient photocatalyst for stable visible water splitting via a two-electron pathway. Science *347*, 970–974.

Mao, Z., Chen, J., Yang, Y., Wang, D., Bie, L., and Fahlman, B.D. (2017). Novel g-C_3N_4/CoO nanocomposites with significantly enhanced visible-light photocatalytic activity for H_2 evolution. ACS Appl. Mater. Interfaces *9*, 12427–12435.

Patnaik, S., Martha, S., Madras, G., and Parida, K. (2016). The effect of sulfate pre-treatment to improve the deposition of Au-nanoparticles in a gold-modified sulfated g-C_3N_4 plasmonic photocatalyst towards visible light induced water reduction reaction. Phys. Chem. Chem. Phys. *18*, 28502–28514.

Sakimoto, K.K., Wong, A.B., and Yang, P. (2016a). Self-photosensitization of nonphotosynthetic bacteria for solar-to-chemical production. Science *351*, 74–77.

Sakimoto, K.K., Zhang, S.J., and Yang, P. (2016b). Cysteine–Cystine Photoregeneration for Oxygenic Photosynthesis of Acetic Acid from CO_2 by a Tandem Inorganic–Biological Hybrid System. Nano Lett. *16*, 5883–5887.

Tang, C., Liu, E., Fan, J., Hu, X., Ma, Y., and Wan, J. (2015). A graphitic-C_3N_4-hybridized Ag_3PO_4 tetrahedron with reactive {111} facets to enhance the visible-light

photocatalytic activity. RSC Adv. *5*, 91979–91987.

Wang, Q., Guan, S., and Li, B. (2017). 2D graphitic-C_3N_4 hybridized with 1D flux-grown Na-modified $K2Ti_6O_{13}$ nanobelts for enhanced simulated sunlight and visible-light photocatalytic performance. Catal. Sci. Technol. *7*, 4064–4078.

Wang, B., Jiang, Z., Yu, J.C., Wang, J., and Wong, P.K. (2019). Enhanced CO_2 reduction and valuable C_{2+} chemical production by a CdS-photosynthetic hybrid system. Nanoscale *11*, 9296–9301.

Xu, M., Tremblay, P.-L., Jiang, L., and Zhang, T. (2019). Stimulating bioplastic production with light energy by coupling *Ralstonia eutropha* with the photocatalyst graphitic carbon nitride. Green Chem. *21*, 2392–2400.

Ye, J., Yu, J., Zhang, Y., Chen, M., Liu, X., Zhou, S., and He, Z. (2019). Light-driven carbon dioxide reduction to methane by *Methanosarcina barkeri*-CdS biohybrid. Appl. Catal. B *257*, 117916.

Zang, Y., Li, L., Xu, Y., Zuo, Y., and Li, G. (2014). Hybridization of brookite TiO_2 with g-C_3N_4: a visible-light-driven photocatalyst for As^{3+} oxidation, MO degradation and water splitting for hydrogen evolution. J. Mater. Chem. A *2*, 15774–15780.